Effect of C Implantation on the Properties of Hexagonal Multi-walled Boron Nitride Nanotubes

By

SYEDA RABAB NAQVI

40-FBAS/MSPHY/F10

Department of Physics
Faculty of Basic and Applied Sciences
International Islamic University, Islamabad
(2012)

i
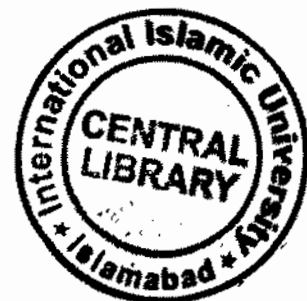
I Boron

II Earthy materials

III Theses

Effect of C Implantation on the Properties of Hexagonal Multi-Walled Boron Nitride Nanotubes
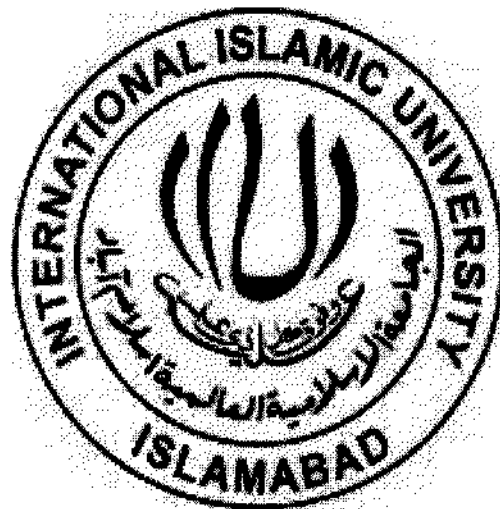
Researcher Name:

Syeda Rabab Naqvi

40-FBAS/MSPHY/F10

Supervisor:

Dr. Javed Iqbal Saggu

Assistant Professor, IIUI

Department of Physics
Faculty of Basic and Applied Sciences
International Islamic University, Islamabad
(2012)

بِسْمِ اللّٰهِ الرَّحْمٰنِ الرَّحِيمِ

In the name of Allah, the Beneficent, the Merciful

International Islamic University, Islamabad
Faculty of Basic and Applied Sciences
Department of Physics

Dated: <u>August 13, 2012</u>

Final Approval

It is certified that the work presented in this thesis entitled "Effect of C implantation on the properties of hexagonal multi-walled Boron Nitride Nanotubes" by **Syeda Rabab Naqvi, Registration No. 40-FBAS/MSPHY/F10** is of sufficient standard in scope and quality for the award of degree of MS Physics from International Islamic University, Islamabad.

<u>Committee</u>

External Examiner

Prof. Dr. Zakka Ullah
Department of Physics
Quaid-e-Azam University, Islamabad

Internal Examiner

Dr. Said Kareem
Assistant Professor,
Department of Physics
International Islamic University, Islamabad

Supervisor

Dr. Javed Iqbal Saggu
Assistant Professor,
Department of Physics
International Islamic University, Islamabad
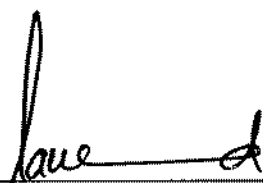
Co-Supervisor

Dr. Ishaq Ahmad
Associate Professor
National Centre for Physics, Islamabad
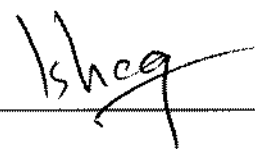
iv

INTERNATIONAL ISLAMIC UNIVERSITY, ISLAMABAD
FACULTY OF BASIC AND APPLIED SCIENCES
DEPARTMENT OF PHYSICS

Effect of C Implantation on the Properties of Hexagonal Multi-Walled Boron Nitride Nanotubes

By

Syeda Rabab Naqvi

(Registration No. 40-FBAS/MSPHY/F10)

A thesis submitted to

Department of Physics

International Islamic University Islamabad for the award of the degree of

MS Physics

Signature: _____

(Chairperson, Department of Physics)

Signature: _____

(Dean FBAS, IIU, Islamabad)

A thesis submitted to

Department of Physics

International Islamic University Islamabad

as a partial fulfillment for the award of the degree of

MS Physics

Declaration

I hereby declare that this thesis work, neither as a whole nor a part of it has been copied out from any source. Further, work presented in this dissertation has not been submitted in support of any application for any other degree or qualification to any other university or institute. If any part of this project is proved to be copied from any source or found to be reproduction of some other project, I shall be legally responsible for punishment under the plagiarism rules of Higher Education Commission (HEC), Pakistan.

Syeda Rabab Naqvi

(40-FBAS/MSPHY/F10)

Dedicated to my father and to my mother,

Who

Brought me to the level

Of

Excellence

I am standing today

ACKNOWLEDGMENTS

encouragement enabled me to complete this research work. I wish to express my special and sincere thanks to **Dr. Shaista Shahzada** Head of Department of Physics, Female Campus, IIUI for her co-operation.

Whatever I am today could never have become true without proper guidance, efforts, and prayers of my parents. Heartfelt thanks are extended to my brothers and sister for their encouragement, keen interest and generous help in conducting research.

I sincerely thank my special friends **Fatima Ali Khan, Hira Shakeel, Ghulam Aisha** and **Hassina Tabassum** for their affectionate behavior, amicable attitude and prayers for my success. I am greatly thankful to my class fellows and friends, who helped me in these endeavors.

MAY ALLAH ALMIGHTY BLESS ALL OF THEM (Ameen).

Syeda Rabab Naqvi

TABLE OF CONTENTS

List of Figures

List of Tables

List of Abbreviations

The following abbreviations are used in the text:

SWNTs	Single-Walled Nanotubes
MWNTs	Multi-Walled Nanotubes
BNNTs	Boron Nitride Nanotubes
h-MWBNNTs	Hexagonal Multi-walled Boron Nitride Nanotubes
EFM	Electric Force Microscope
STM	Scanning Tunneling Microscope
C^+	Carbon ion
$°C$	Degree Celsius
UV	Ultravoilet-Visible
CNTs	Carbon Nanotubes
TPa	Tera Pascal/ 10^{12} Pascal
W/mK	Watt per milli Kelvin
Å	Angstrom / 10^{-10} meter
BCN	Boron Carbonitride
HRTEM	Higher Resolution Transmission Electron Microscope
SEM	Scanning Electron Microscope
SHS	Self propagation High temperature Synthesis
XRD	X- Ray Diffraction
NRBS	Non- Rutherford Backscattering Spectroscopy
IR	Infrared
ATR	Attenuated Total Reflections
eV	Electron Volt
HVEM	High Voltage Electron Microscope

CCD	Charge-Coupled Device
nm	Nanometer/ 10^{-9} meter
Hz	Hertz
kJmol^{-1}	Kilo Joule per mole
CVD	Chemical Vapor Deposition

Abstract

Hexagonal Boron Nitride Nanotubes (h-BNNTs) have emerged as an analogue to carbon nanotubes. Only the difference is that here boron and nitrogen atoms alternatively replace carbon atoms. These nanotubes are composed of one atom thick sheets of boron nitride honey comb structure. These nanotubes are as versatile as their C counterpart, with quite different physical properties due to different elemental components. Boron Nitride (BN) and Carbon (C) systems have almost the same lattice parameters, which makes it possible to construct B-C-N nanostructures. This hybrid ternary B-C-N structure is demonstrated to exhibit the electrical behavior which lies midway between h-BN and C lattices. Moreover exposure of BNNTs to energetic particle beams is an important and standard tool for modifying material properties.

In this research work, hexagonal multi-walled boron nitride nanotubes were doped with carbon atoms by 0.8MeV C^+ ions irradiation. This doping is proposed to be substitutional, as carbon atoms replace B and N atoms at different lattice sites. Results of transmission electron microscopy (TEM) revealed structural transition from hexagonal to amorphous BN structure. More over nanotubes junctions were observed by scanning electron microscopy (SEM). At a dose of 10^{12}ions.cm^{-2} and 10^{13}ions.cm^{-2}, amorphization is less prominent but it increases with increasing ion dose. Different characterization techniques were employed to confirm the Carbon doping in Boron nitride honeycomb lattice. X-Ray diffraction was used for structural investigation. Raman spectroscopy, non-Rutherford backscattering spectroscopy (NRBS) and Infrared (IR) spectroscopy were used to study effects of C implantation on nanotubes. X-Ray Diffraction (XRD) results show that after ion implantation an additional peak becomes visible at $2\theta = 41.9^0$, which could be attributed to h-BCN (100) plane. B-C-N Raman optical mode peak appear after 0.8MeV C^+ ions irradiation. Infrared Spectroscopy confirms that in ion implanted nanotubes, boron and nitrogen atoms form bonds with carbon atoms, hence B-N, B-C-N, B-C and C-N bonds are observed in the spectra. C Implantation in h-BNNTs is proposed to the knockout ejections of B and N atoms by high energy C^+ ions and consequently make ternary B-C-N structure. Ultravoilet-visible absorption spectroscopy of irradiated and un-irradiated BNNTs revealed that band gap decreases with an increase in ion dose.

Materials in B-C-N triangular zone are most efficient materials and are known as Frontier carbon materials. Hence C implantation is a successful technique for tuning the band gap of BNNTs and making them efficient materials for nanoscale engineering.

CHAPTER 1

1. Introduction

1.1 Nanoscience and Nanotechnology

The term Nanotechnology was used by late Norio Taniguchi (University of Tokyo) in 1979 for the first time, referring to precise engineering of materials at such a miniscule scale [1]. Nanoscience is an emerging field of science which is concerned with the study of materials having very small dimensions, in the range of 10^{-9}m [2]. It is sometimes considered as structural fabrication, design of devices and control over the properties at nanometer size, therefore the heart of nanotechnology is control of size with desired properties [3].

Nanotechnology is sometimes referred to be new, but it is not new because it is the only field which is concerned with phenomena related to atoms and molecules. In different ways, the disciplines of science are dealing with relationships between atoms and molecules and their behaviors. Quantum mechanics defines absolute smallness, thus to understand the properties at nanoscale quantum physics is important, for example the study of atomic clusters named as quantum dots or nanoparticles [3].

1.2 Nanoscience and Physics

Physics being the mother of all natural sciences can be used to explain every phenomenon that occurs at the nano scale. Here one manipulates individual atoms and molecules rather than working on bulk scale. Therefore physicists have focused research in the field of nano-mechanics, quantum teleportation, quantum computation, artificial atoms etc. Physics at the nanoscale is very different. At such a scale some properties not seen on a macroscopic scale become important and a change in quantum mechanical and thermodynamic behavior is observed. We need to know the properties of individual molecule and we manipulate them in a well-defined manner to produce new materials with amazing characteristics [2].

1

1.3 Classification of Nanomaterials

Nanomaterials have outclass thermal, mechanical and electrical properties and these properties make them ideal for applications in electronics, photonics, medicines and other environmental applications.
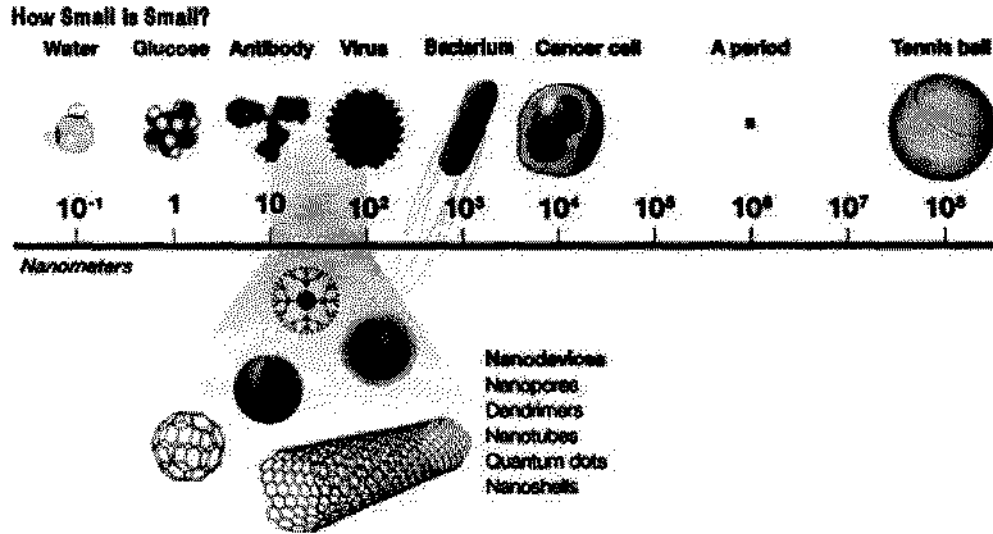
Figure 1.1: A view of nanometer size [2]

Table 1 Classifications of Nanomaterials on the basis of dimensionality [2]

Classification	Confinement	Examples
2 dimensional	1 dimension < 100nm	Membranes and thin films etc.
1 dimensional Zero dimensional	2 dimensions < 100nm	Nanorods, nanowires, nanotubes, fibers, Platelets, etc.
	3 dimensions < 100nm	Particles, quantum dots, hollow Spheres, etc.

2

1.4 Nanotubes

Nanotubes fall in the category of nanomaterials, known as one dimensional. Their two dimensions are confined to the nanoscale. These systems contain layers of atoms seamlessly wrapped to form cylindrical structures. Their diameter is only a few nano-meters, yet they can be up to milli-metres long. Their aspect ratio the (length-to-width ratio) is extremely high [4]. Nanotubes can be made of organic or inorganic materials. In Figure 1.2 an example of single walled nanotube is shown.

Nanotubes are the strongest materials available on the earth. Depending on the type of atoms, different nanotubes show different useful properties. Such useful properties include electronic, thermal, mechanical and optical behaviors. Constituents of the nanotubes can be different atoms like carbon or boron nitride.
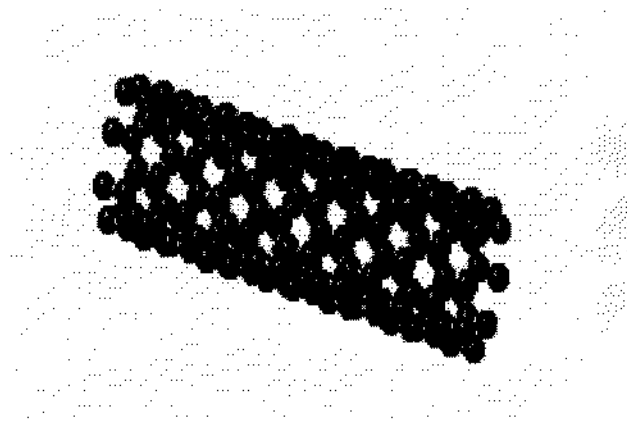
Figure 1.2: single-walled nanotubes [5]

1.4.1 Types of Nanotubes

A nanotube can be single-walled or multi-walled. Former is the cylindrical structure consisting of a single sheet of atoms, known as Single-Walled Nanotubes (SWNTs). Multi-walled nanotube (MWNTs) consists of concentric cylinders nested like rings of a tree trunk, here a tube of smaller radius lies inside the tube of larger radius. Example of both types of nanotubes is shown in Figure 1.3
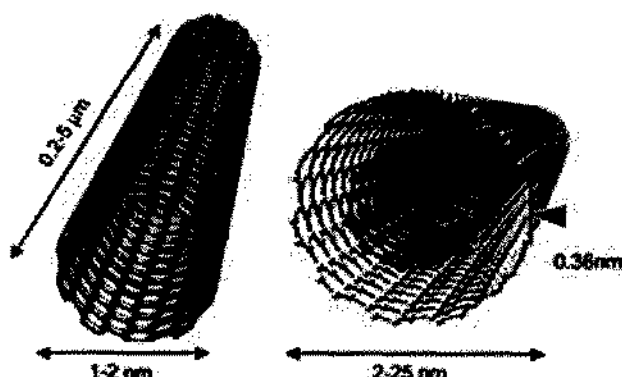
Figure 1.3: Single-walled nanotube (SWNT) and multi-walled nanotube (MWNT) [6]

According to rolling convention of the sheet of atoms, nanotubes are classified as armchair, chiral and zigzag nanotubes. When the sheet of atoms is rolled along one of the symmetry axis, zig-zag or armchair nanotubes are formed. Chiral nanotubes are formed when the equivalent atoms of each unit cell are aligned on a spiral (Figure 1.4).
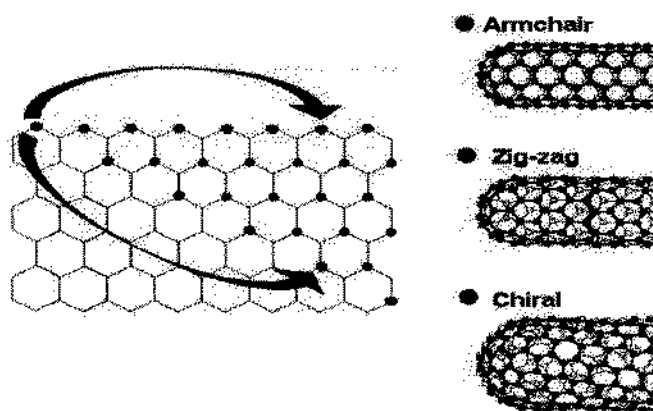
Figure 1.4: Types of nanotubes based on rolling convention [7]

Properties such as strength, thermal conductivity, density and electrical conductance are influenced by these structural differences. According to their structure, some of the nanotubes are metallic and some are semi-conductor. Furthermore depending on their growth mechanism and material composition, nanotubes can be synthesized with open or closed ends [8].

1.4.2   Carbon Nanotubes(CNTs)

A carbon nanotube is one of the most popular types of nanotube. It is a cylindrical structure which either has single wall or multi walls of graphite atoms. Their diameter is about 1-3 nanometers and length ranges between hundreds to thousands of nanometers. Thus a single-walled carbon nanotube (SWCNT) can be imagined as a single graphene sheet rolled in a cylindrical shape. Similarly a multi-walled carbon nanotube (MWCNT) can be thought of as an assembly of concentric cylindrical SWCNTs. The distance between these tubes is approximately same as the distance between graphene sheets in natural graphite. Thus carbon nanotubes are well-defined cylindrical structures [5].

In 1991 Sumio Iijima, a Japanese scientist discovered multi-walled carbon nanotubes by using arc discharge method. Outer diameter for these tubes ranged between 3 nm to 30 nm. He used two graphite rods as electrodes and electrical sparks were passed between them to vaporize them and carbon was allowed to condense to get product. Tiny tubes of carbon called multi-walled carbon nanotubes were formed with many layers instead of expected C_{60} product [9, 10]. Two years after the discovery of multi-walled structure, transition metals used in the arc discharge method resulted in the formation of single-walled carbon nanotubes [11, 12].

Carbon nanotubes are mainly produced by chemical vapor deposition (CVD) method. Moreover laser ablation and arc-discharge methods are used in common. In CVD method, the catalyst is heated in a high temperature furnace under a hydrocarbon gas atmosphere and the products are collected over the catalyst. On the other hand, laser ablation apparatus is consists of target material, furnace, laser apparatus and water cooled collector [13].

1.4.3 Properties of Carbon Nanotubes

Carbon nanotubes are ideal AFM probes due to superb mechanical properties and high aspect ratio. Faithful imaging of deep trenches is possible due to their high aspect ratio. Similarly their diameter is at the nanoscale which makes it possible to retain high resolution [14]. Nanotubes exhibit buckling when put under torsional, compressive or bending stress, which is due to their hollow structure. Although CNTs are durable,

flexible and strong yet they tend to undergo buckling rather than breakage when deformed. This behavior results in highly robust probes [14]. Their tensile strength values vary from 10 to 150GPa and Young's modulus ranges from 0.27 to 4.15TPa. Average Young's modulus value is reported as 1.8TPa. Tensile strength value is 60GPa for a single perfect nanotube. For MWCNTs tensile strength has sufficiently higher value i.e, 150GPa. Strength of CNTs is 100 times greater than steel although steel is 6 times heavier than CNTs [15]

Carbon nanotubes exhibit interesting electrical behavior. This electrical behavior depends on many factors such as, the way the graphite structure spirals around the tube. Armchair CNTs are metallic similarly zigzag carbon nanotubes are semiconducting or metallic. Electrical behavior of MWCNTs is quite similar to the SWCNTs. Electrical properties are influenced by some other factors like doping etc. Carbon nanotubes (NT) are ready-made molecular wires for transistors applications. These properties can be rendered into an insulating, semiconducting, or conducting state, which make them ideal for future nanocomputer design. Carbon nanotubes have prospective thermal, electrical, and selective-chemistry applications [5, 14].

CNTs exhibit excellent thermal conductivity, at room temperature it is about 6000 W/(m.K). Such a high thermal conductivity proves them to be a good thermal conductor. Their thermal stability is about 750^0C in air and 2800^0 C in vacuum [16].

1.4.4 Applications of Carbon Nanotubes

Carbon nanotubes have many potential applications. These applications include conductive composites offering excellent mechanical properties. Moreover devices which can store and convert energy and sensors are probably the most important applications of nanotubes. Interconnections at the nanoscale and semiconductor devices are another important outcome of nanotube engineering. Probes, radiation sources and hydrogen storage are some other applications of CNTs. Some applications of CNTs are being utilized in industries and others are also expected to have potential uses [17]. Carbon nanotubes have many application areas in material science and engineering, as well as in biotechnology, electronics, pharmaceuticals, medicine. This is due to their excellent

thermal conductivity, high tensile strength, high Young's modulus and electrical properties.

CNTs have wide applications in electronic industry. Semi conducting behavior of CNTs is quite better as compared to silicon. Semi-conductive carbon nanotubes are efficiently used for production of field effect transistors. Conductive CNTs are used as the constituent of the tips of electric force microscopes (EFM) and scanning tunneling microscopes (STM) [15]. Good thermal conductivity and large surface area of carbon nanotubes, proves them to be good catalyst supports in fuel cells and as electrodes in batteries. Their role is very dominant in hydrogen storage in fuel cells [16]. Other applications of CNTs include solar cells, artificial muscles, clothes, filters, computers, sports equipment like tennis rackets, golf balls etc and displays [18].

1.5 Boron Nitride and Similarities between Hexagonal Boron Nitride and Graphite

Discovery of carbon nanotubes was not an end, it was a gateway to the discovery of other nanostructures. Researchers started to work to find other possible nanotubes. Boron nitride is one of those nanostructures. Boron nitride molecule is the combination of boron and nitrogen atoms. Due to different atomic arrangements of boron and nitrogen atoms, crystal structures of boron nitride fall in three catagories namely hexagonal, cubic and rhombohedral (Figure 1.5).
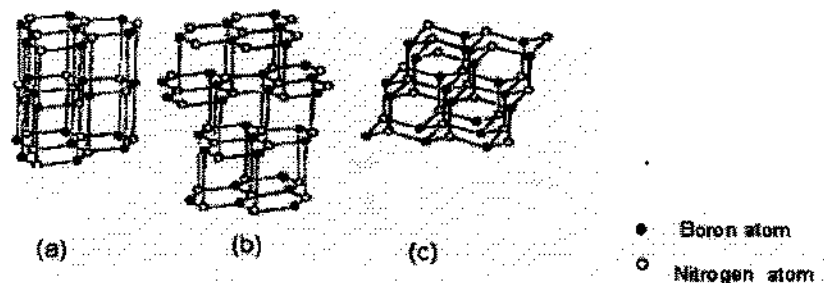
Figure 1.5: Boron nitride crystal structures: (a) hexagonal, (b) rhombohedral (c) cubic [19]

When hexagonal BN is treated at high temperature and pressure, cubic BN is produced. It is used as a tool cutter due to its extensive hardness. It is an electrical insulator and a

good conductor of heat. It has high value of thermal conductivity. The cubic phase of boron nitride is the only material whose strength is comparable to that of diamond. It has structural similarity with diamond. Rhombohedral boron nitride is quite similar to hexagonal form of boron nitride (h-BN). Hexagonal BN has a structural similarity with graphite and it is known as white graphite. In air it is stable up to temperatures of 1000^0C, up to 2800^0C under inert atmosphere, and up to 1400^0C under vacuum. The hexagonal structures of Graphite and BN are shown in Figure 1.6. They have almost equal crystallographic parameters. Their bond lengths are almost similar. In other words both of these hexagonal structures are almost identical. When temperature and pressure is kept high, both graphite and boron nitride are found in liquid phase. At high pressure, these materials become ultra hard [20, 21].
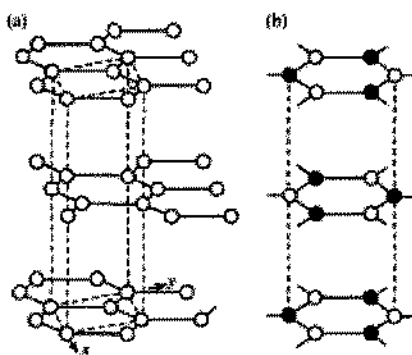
Figure 1.6: Hexagonal structures of graphite and BN [22]

1.6   Boron Nitride Nanotubes (BNNTs)

The most well known crystal structure of boron nitride (h-BN) contains ABAB stacking and belongs to the D^4_{66} point group. In contrast with graphite, B(N) atomic layer lies vertically above the N(B) atoms, where as in case of carbon, one atom in each pair lies exactly above the center of hexagon. Such a stacking geometry confirms that B-N is a very strong ionic bond. The comparison of bond lengths of both the B-N and C-C bond depicts that the bond length in h-BN is greater than that in graphite (as α_{cc} = 1.42 Å and α_{BN} = 1.45 Å) [23].

Nanotubes have outclassed properties and they can be made of a variety of materials. Hexagonal boron nitride (h-BN) is a graphite-type structure. It is a layered material with

8

regularly stacked planar networks of BN hexagons. In 1994, prediction of hexagonal boron nitride nanotubes was theoretically presented for the first time. Since the structure of graphite and white graphene is similar thus the idea of synthesis of boron nitride nanotubes was extracted from this logic and on the basis of this idea theoratical prediction was established. Synthesis process was successfully achieved in 1995. As a structural analogue of carbon nanotubes (CNTs), BNNTs have emerged as the most versatile inorganic nanostructure [23].
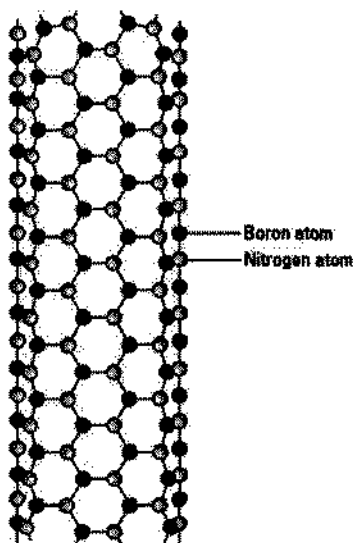
Figure 1.7: Hexagonal Boron Nitride nanotube [24]

Boron nitride sheet can be rolled into cylindrical structures using different rolling conventions to form zigzag, armchair and chiral BNNTs.

1.6.1 Properties of Boron Nitride Nanotube

Accurate ab-initio calculations showed that an isolated BN sheet can be rolled with almost equivalent elastic energy, as that required for rolling a layer of carbon atoms arranged in honeycomb convention, provided the radius of nanotube is same for both the cases.

9

Table 2 Properties of BNNTs in terms of Chirality (n, m) [23]

Symbolic Representation	Name	Mathematical Expression	Value
(a_1, a_2)	Basic vectors	$a\left\{\sqrt{\dfrac{3}{2}}, \pm\dfrac{1}{2}\right\}$	{x,y} cartesian
(b_1, b_2)	Reciprocal Lattice vectors	$\left\{\dfrac{1}{\sqrt{3}}, \pm 1\right\} 2\pi/a$	{x,y} cartesian
A	Lattice constants	$a = \sqrt{3}\ \alpha_{BN}$	α_{BN}= 1.45 Å
d_r	Tube diameter	$d_r = \dfrac{a}{\pi}\sqrt{n^2 + nm + m^2}$	$0 \leq |m| < n$
C_h	Chiral vector	$C_h = na_1 + ma_2 = (n, m)$	$0 \leq |m| < n$

The electronic behavior of BNNTs is different from CNTs. Carbon nanotubes are either semi-conductive or metallic. Boron nitride nanotubes are insulating systems. As the B-N bond is strong ionic bond, thus nanotubes possess a wide energy gap, which is greater than 5eV. This bandgap is independent of tube radius and helicity.

Tight binding model successfully explains large energy band of BNNTs. This model is mostly considered for graphitic lattice, its validity is around the fermi state. Here a single p_x orbital is considered for each atom. Z-axis is always taken along the normal to graphene sheet. Here we consider that $E_{A(B)}$ is the value of energy which is onsite for A(B) atoms. Similarly γ is the value of energy due to overlap of neighboring orbitals. In order to determine electronic character, we need to write electronic eigen states. The electronic states in BNNTs for A/B atoms, can be expressed in Bloch basis:

$$\varphi_k(r) = C_A P_k^A(r) + C_B P_k^B(r) \tag{1.1}$$

Where energy eigen function of Bloch basis $P_k^{A/B}$ is expressed as a product of plane wave envelope function and periodic Bloch function.

$$P_k^{A/B} = 1/\sqrt{N} \sum_R e^{ik.R} P_z(r - \tau_{A/B} - R)$$

Here k stands for plane wave vector, N for number of primitive cells in the crystal and R for lattice vector. $\tau_{A/B}$ is a parameter which belongs to atomic positions. For this type of basis, energy dispersion relation derived from secular equation is given by

$$E(k) = \pm \gamma \sqrt{(\Delta/4\gamma)^2 + \propto (k)^2} \tag{1.2}$$

$$\text{with: } \Delta = E_A - E_B$$

and $$\propto(k) = \gamma \sqrt{1 + 4\cos(k_x a \sqrt{3/2}) \cos(k_y a/2) + 4\cos^2(k_y a/2)} \tag{1.3}$$

Periodicity of the reciprocal lattice vector is denoted by K, mathematically it is verified that $\propto(k)$ vanishes for $k = K$. As graphene sheet contains carbon atoms at each atomic site thus for any two atoms $E_A = E_B$ at boundry of the Brillouin zone and $\Delta = 0$. This result explains the semimetallic behavior of graphene sheet. Hence the band gap closing is observed at the corners of Brillouin zone. Where as electronic behavior of h-BN is quite different. Here both the neighboring atoms are not same, hence $E_A - E_B \neq 0$. When $k = K$, the energy gap takes a value of $E_{BN(k=K)} = 2\Delta$, thus even at the corners of Brillouin zone, band gap does not close. It can be concluded from above discussion that band gap of boron nitride honey comb lattice does not depend on the atomic structure. As $\propto(k)$ is not important in this regard, which is a parameter related to hopping strength γ and crystallographic structure. This explains the fact that why band gap of h-BN nanotubes is "stable", which is independent of helicity and curvature. But the statement may not be true for the tubes of very small radii [25, 23].

Boron nitride nanotubes (BNNTs) are strongly polar due to presence of large charge on boron and nitrogen atoms which are alternatively arranged in the honeycomb lattice. Hence electrostatic interactions are important to consider while studying the elastic behavior of h-BN lattice. Elastic properties BNNTs were studied by varying the partial atomic charges on boron and nitrogen. Similarly in case of multi-walled nanotubes, Young modulus (Y) and Shear modulus (G) were calculated by using mechanics at the molecular scale and effect of number of walls and tube radii on these properties was observed. The elastic modulus of BNNTs was reported as 6 times greater than that of

CNTs. Young modulus of BNNTs was found to increase with an increase in magnitude of the partial atomic charge on boron and nitrogen atoms. Young modulus of BNNTs can be larger than the Young modulus of CNTs of same radius [26].

Theoretical and experimental studies have revealed that BNNTs are good conductors of heat. Because phonons very actively participate for transfer of heat in boron nitride nanotubes. BNNTs are potential nano-fillers for insulating composite materials since they preserve the insulation yet lead to high thermal conductivities.

BNNTs possess many other excellent properties including chemical inertness and surface polarizibility. These are structurally more stable than CNTs and offer a high resistance to oxidation. Due to these outstanding properties, BNNTs have become an important part of industry [27].

Comparison of properties of BNNTs and CNTs is listed in below (Table 3). It is observed that BNNTs are better than CNTs in their mechanical behavior. Similarly chemical properties of BNNTs are better than that of CNTs. However, CNTs are thermally more conductive as compared to BNNTs.

Table 3 Comparison of properties of CNTs and BNNTs

Properties	BNNTs	CNTs
Electronic Properties[28]	Always Semiconducting	Metallic/ semi conducting
Young's Modulus(TPa)[29]	1.22± 0.24	1.8
Oxidation Temperature (^{0}C)[30]	800-900	400
Thermal Conductivity(W/mK) [31]	High value expected Hexagonal boron nitride : 600 W / m K [in ab plane][31(a)]	More than 3000 W / m K[31(b)]

12

1.6.2 Properties of Boron Carbonitride Nanotubes (BCNNTs)

Doping of carbon in boron nitride nanotubes (BNNTs) results in the formation of boron carbonitride nanotubes (BCNNTs). This relatively new material has become a hotspot of international material science. Due to similarity of crystalline structure and contrast of electrical properties of CNTs and BNNTs, it is possible to obtain ternary graphite-like BCN nanotubes, which exhibit adjustable semiconducting properties by modifying the ratio C: BN [32].
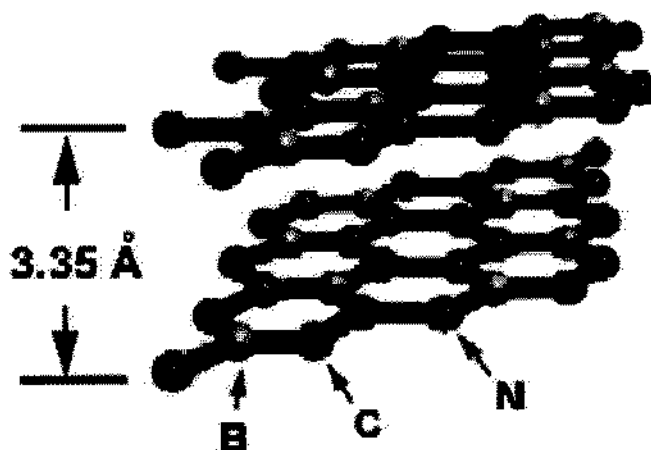
Figure 1.8: Theoretical model of BCN layer [33]

As we keep on increasing the carbon content in BNNTs, a newly derived energy band appears around the center of bandgap of BNNTs. Newly derived energy band belongs to C atoms, which effectively reduces the band gap of BNNTs. Moreover this doping could apparently reduce electrical resistance of parent material [34-39]. Carbon doping in Boron nitride lattice is supposed to induce spontaneous magnetism and thermal stability is drastically increased. Such carbon doped Boron nitride nanotubes are also known as boron carbonitride nanotubes (BCNNTs). BCN nanotubes exhibit semiconducting behavior which can be tuned with the quantity of carbon content. BCN nanotubes offer good lubrication and intercalation properties. These nanotubes share their physical properties with BN and C systems, having a large young's modulus up to 1.2Tpa and are resistant to oxidation up to 1173K in air [40, 41].

13

1.6.3 Applications of Boron Nitride Nanotubes

Researchers are trying to find new application areas for BNNTs. Having outstanding properties makes them suitable for many applications in which CNTs were previously used. BNNTs are used for hydrogen storage. Their hydrogen storage capacity is better than CNTs. Because in BN honeycomb lattice, boron and nitrogen offer more attraction to hydrogen molecule as compared to carbon in CNTs. Hydrogen storage capacity increases with an increase in nanotube diameter [42]. In atomic force microscopy (AFM), boron nitride nanotubes are used as a nano-probe to improve the resolution of the image. Due to its excellent mechanical, electrical and chemical properties, BNNTs are good candidates for producing composite materials. BNNTs are being studied for a wide array of prospective applications, such as high-temperature lubricants, high-temperature transistors, photo luminescent devices, flat-panel displays and reinforcements for weaker materials [43].

As already mentioned, BNNTs offer high resistance to oxidation than CNTs, so they are useful for high temperature applications in which CNTs would certainly burn. Moreover Carbon doped BNNTs can work more efficiently in high temperature environments. Boron carbonitride nanotubes (BCNNTs) are important for environmental and industrial applications. Such doped nanotubes are expected to have potential applications in electrical conductors, electronics, novel composites and high temperature lubricants. Being a new material for selective adsorption of CO_2, they can be used in gas sorption applications as well [44].

1.7 Literature Review

Hexagonal multi-walled boron nitride nanotubes are insulators or semiconductors with high band gap. Their usefulness depends on tunability of band gap so that nanotubes can be efficiently used in optoelectronics and photonics. BNNTs doped with a small amount of carbon can be made semiconducting with the appearance of dopant or defect state in the band gap of nanotubes. As concentration of dopant increases, a crossover from insulating to metallic is observed. Although boron carbonitride nanotubes are better as compared to carbon and Boron nitride nanotubes, but they are difficult to synthesize [40].

14

Carbon doped boron nitride is useful for nano-engineering as they offer a high resistance to oxidation. They can be effectively used at high temperature as nanotransistors. BCNNTs are photoluminescent materials and offer lubrication properties [36]. Boron nitride nanotubes were prepared for the first time by Chopra et al by using arc discharge method. During this process, boron nitride powder was encapsulated in a tungsten electrode [51]. A modification to this synthesis technique was introduced by Loiseau et al and Terrones et al. They used arc discharge method which resulted in the formation of nanotubes with square-like tip ends and caps having encapsulated metallic particles. Particularly, HfB_2 electrode produced BNNTs with less number of walls. Most common morphologies were single-walled and double walled nanotubes having square-shaped closed caps [52-53]. Golberg et al have a major contribution in the production of BN nanostructures by laser ablation technique. Laser ablation of hexagonal or cubic BN targets was performed at very high pressure of nitrogen(up to 15GPa). A bulk quantity of small multi-layered BNNTs was prepared with a surface temperature $5000^{\circ}C$ of BN target. After the successful synthesis of BNNTs, efforts were devoted toward the synthesis of ternary BCN nanotubes. In 1994, synthesis of BCN nanotubes was reported for the first time [54].

Composite nanotubes of varying morphologies were prepared by Stephen et al. He used electric arc discharge method, in which cathodes were made up of graphite and anodes were in the form of amorphous boron-filled graphite. Synthesized composite material contained carbon, boron and nitrogen species. Process was carried out under nitrogen atmosphere. One-to-one ratio of boron and nitrogen atoms was confirmed from electron energy loss spectra. It was suggested that boron and nitrogen substitute carbon in the graphitic lattice. Studies revealed that single phase $C_yB_xN_x$ and separated domains (nanosize) of BN may exist in carbon networks [38]. Synthesis techniques commonly employed for BCN nanostructures are laser ablation, Chemical vapor deposition(CVD) and arc discharge which are same as used for the synthesis of carbon nanotubes.

Pyrolisis of hydrocarbon precursors over metal catalysts is also used for the synthesis of BCN nanotubes. Wengsieh et al prepared BCN nanotubes in helium atmosphere by arc

discharge method. Graphite anode with encapsulated BN was used in the process, whereas cathode was pure graphite [55].

Zhang et al synthesized BCN nanotubes by method of laser ablation. During the process target was a composite material having BN, C, Ni and Co at 1000°C, that was kept under N_2 atmosphere.

Terrones et al performed the pyrolysis of $CH_3CN.BCL_3$ over a Co powder at 1000°C to prepare BCN nanotubes. BCN nanotubes synthesized with above mentioned methods were obtained with varying morphologies. For preparation of nanotubes in bulk, chemical vapor deposition was developed. Nanotubes were obtained in large quantity (e.g, tens of grams) with relatively low cost. Sen et al used catalytic pyrolysis method for the efficient synthesis of BCN nanotubes with different compositions. Materials containing BCN in different quantity were subjected to catalytic pyrolysis at suitable temperature range (ca 600-1200 $^{\circ}$C) [56].

Kohler-Redlich et al prepared stable BC_2N nanotubes by pyrolysis of $CH_3CN.BCL_3$ over Co at 1000°C. The nanotubes exhibited stacked cone sub-units roughly aligned along the direction of tube axis. Co nanoparticles were encapsulated at the tips. Stichiometric studies were performed by electron energy loss spectroscopy (EELS) which depicted BC_2N stichiometric composition of BCN nanotubes. BCN materials have been composed by means of laser ablation, CVD and arc discharge method. During such synthesis processes BN and C layers with separated phases were obtained [60].

M. Terrones et al obtained B_4CN nanocrystals and B doped carbon nanotubes by using arc discharge method. Anode was made up of a composite material, particularly BCN. B or BN powder filled graphite electrodes were evaporated during the process. Higher concentrations of BN or B contents were possible to synthesize during this experiment. Alternatively, BC_xN nanotubes were obtained by pyrolisis of organic precursors over metal catalysts. This technique was found to be better than arc discharge method for the production of BC_2N in the uniform range of stichiometric composition [57].
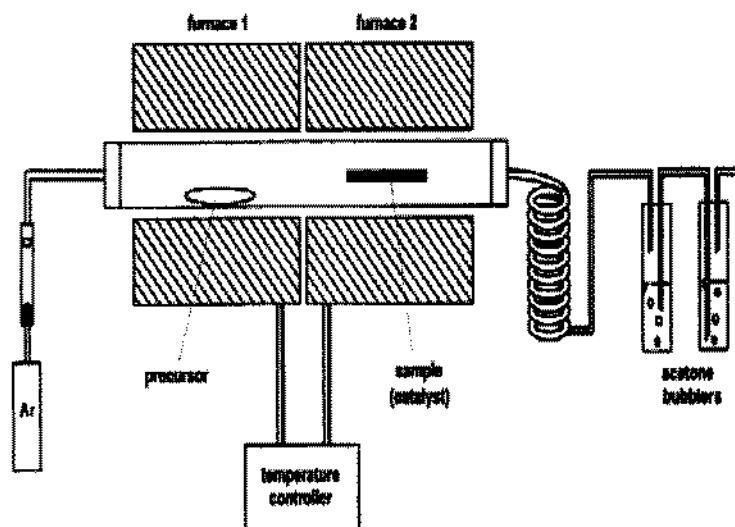
Figure 1.9: Experimental setup for pyrolisis [57]

Liao et al used bias assisted hot-filament CVD method for the synthesis of massive junctions between carbon nanotubes and boron carbonitride nanotubes. They used clean wafers of nickel as a substrate and discharge plasma glow was produced by dc power supply. A tantalum anode was installed above a carbonized tungsten filament. A continuous CVD method involving two-step growth was used for the synthesis of C/BNC junctions. First, the flow rates of N_2, H_2 and CH_4 were kept at 75, 5 and 20 sccm, respectively. Growth process started at a pressure of 2.0 kPa when filament temperature was $1600^{\circ}C$ and a voltage of 600V was applied to produce glow discharge plasma. Growth process continued for 10 minutes which caused a decrease of $1500^{\circ}C$ in the filament temperature. Later on, B_2H_6 gas was entered into the chamber with a concentration of 5 vol %. With this method multi-walled boron carbonitride nanotubes were grown on the surface of carbon nanotubes, and C/BNC nanotube junctions were formed with a sharp interface [40].

Koos et al used a 'standard' aerosol CVD method in conjunction with triethylborane, benzylamine, toluene and hexane mixtures. With this technique carbon nanotubes were synthesized with varying concentrations of boron and nitrogen. Precursors were decomposed at a high temperature $(800^{\circ}C-1100^{\circ}C)$ under argon at atmospheric pressure. Concentration of boron and nitrogen content of carbon nanotubes could be controlled

between 0–2.2 and 0–0.5 at.% respectively. A typical laboratory-sized 50 cm long tube furnace was used to achieve yields between 0.3 and 1.5 g of nanotubes/10 min with a relatively easy approach. Experiments revealed that doping with heteroatoms, such as boron and nitrogen can be used to control the diameter of carbon nanotubes [42]. He et al used a chemical process for the synthesis of single phase crystalline B-C-N compound. Boric acid and melamine were used in the reaction. A mixture of boric acid and melamine was prepared in an agate mortar. For the synthesis of BCN nanotubes, mixture components were added in different ratios. This mixture was heated in a beaker at 200^0C for 1h and then at 300^oC for an additional 2h. After cooling, the obtained B-C-N precursor was pulverized and then kept in a ceramic tube. The sample tube was pushed into the furnace in N_2 atmosphere. This was a successful technique for synthesis of BCN nanotubes with lattice parameters a= 0.251 nm and c= 0.666 nm [43].

Piaza et al synthesized boron carbonitride nanotubes by in situ grown carbon nanotubes. They prepared nanotubes by arc discharge method using a compound anode prepared by pressing high-purity amorphous B powder into a 2.5mm hole   diameter   made in a high-purity 5mm diameter graphite rod. Cathode in the form of a high purity graphite rod 5mm in diameter was mounted on a linear displacement manipulator. The discharge was ignited in high purity N_2 at 400 Torr. Initially electrical contacts were made with electrodes in order to induce resistive heating with a current of ~500A. Heated electrodes emitted an orange glow at a temperature of ~ 900° C. This effect was measured with an optical pyrometer. After reaching this temperature, spontaneously a gap opened between electrodes. This gap was kept constant by displacing cathode. A potential drop accross electrode was varied from 20 to 55 V to maintain the DC current between 50 to 100 A. Products deposited on the cathode were collected that were in the form of a dark-grey filamentous material [44].

Zhi et al used hot- filament chemical vapor deposition (HFCVD) system for synthesis of boron carbonitride nanotubes [45].L. Luo et al synthesized BCN nanotubes with relatively simple and very efficient method. Nanotubes were collected directly onto a commercial stainless steel foil. Growth mechanism was proposed to be vapor-liquid-solid

(VLS) for this technique. In this technique, raw materials of zinc oxide powder, boron powder and ethanol absolute were used [46].

Suenaga, et al prepared tubular and polyhedral graphitic nanoparticles comprised of boron nitride (BN) and carbon layers. Hafnium diboride rod was arced with graphite under nitrogen atmosphere. Nanoparticles were obtained from the soot collected on anode deposit. Products were studied at subnanometer-scale resolution and their elemental studies revealed phase separation between carbon and BN layers along the radial direction. Most of the nanotubes prepared by this method were having a different structure in which a few layers of BN were sandwiched between carbon layers. Carbon layers are found at the periphery and at the center. Ternary boron-nitrogen-carbon system thus obtained was proposed to be useful in nanoscale electronic devices [47].

Wang et al used bias-assisted HFCVD process for direct synthesis of single-walled boron carbonitride nanotubes in bulk quantity. These ternary nanotubes were grown over the powder Fe-Mo/MgO catalyst by using CH_4, B_2H_6, and ethylene diamine vapor as reactant gases. Incorporation of boron content can be achieved within the range of 2-4 atom% and boron content can be as high as 16 atom% in nanotubes [49]. Carbon doping in Boron nitride nanotubes was previously obtained by different chemical synthesis techniques as discussed above. Wei et al introduced substitutional doping of carbon in the boron nitride lattice by electron beam irradiation. Electron beam irradiation gave rise to ejections of boron and nitrogen atoms from honeycomb BN lattice due to bombardment of electrons. This process was accomplished inside an energy filtering high resolution TEM equipped with scanning tunneling microscope (STM)-TEM Nanofactory instrument holder. Already synthesized BNNTs were placed inside TEM. These pure BNNTs were prepared by induction heating method. A source of carbon in the form of a small quantity of paraffin wax (C_nH_{2n-2} with $19 \leq n \leq 36$) was deliberately introduced into the column of TEM. Carbon source was placed at a distance of several millimeters from BN nanotubes. Hydrocarbon molecules diffuse and adsorb on the surface of nanotubes due to introduction of paraffin wax. Electron beam irradiation breaks hydrocarbon molecules and gives birth to free C species [50]. Post synthesis carbon doping in boron nitride as well as chemical synthesis of BCN nanotubes has been previously obtained by different

techniques but these techniques raise the issues of processibilty, stability and lack of control on dopant concentration [50].

1.8 Motivation and Objective

BNNTs were previously doped using different techniques. In most of the literature surveyed, boron carbonitride nanotubes were chemically synthesized. Only one case of post synthesis doping is reported upto now [60]. Also, there is no study which was based on ion implantation technique which is simple as well as provides the benefits of stability, processibilty and control of dopant concentration. In other words, in none of the published studies, such an efficient and easiest approach was reported. Hence this research work aims to report an important feature of BNNTs which is tunability of properties to the desired level. This thesis aims to give an easy approach to get control over the electronic and optical properties. Nanotubes obtained by this methodology offer well defined characteristics. Further characterizations and studies can definitely help to explore and widen the application area of white graphene materials. BCNNTs obtained with this technique can be exploited for the use in gas sensors, electronics, optoelectronics and composite materials industry.

As described earlier, energy band engineering of hexagonal multi-walled Boron nitride nanotubes by ion implantation technique was not experienced in the past. There is not any published information in the literature related to effects of ion irradiation on Boron nitride nanotubes, their structural and spectrometric transitions. Here is objective of our research work

- To prepare samples of as-synthesized BNNTs and placement in 5-UDH Tandem accelerator.
- To control substrate temperature and providing C^+ ions for irradiation.
- To apply sufficient ion dose and ion energy for ion implantation.
- To investigate the influence of ion dose on the structure of BNNTs by HRTEM and SEM studies.
- To confirm doping by non-Rutherford backscattering spectroscopy.
- To characterize the products using XRD, FTIR and Raman spectroscopy.

- To get information about electronic behavior of synthesized boron carbonitride nanotubes by UV-spectrophotometry.

CHAPTER 2

2 Methodology

In this research work ion implantation of hexagonal multi-walled boron nitride nanotubes (h-BNNTs) is performed by using Pelletron tandem accelerator, model 5-UDH. Boron nitride nanotubes were synthesized by using Self Propagation synthesis at high temperature (SHS). Self propagation synthesis and annealing is a process in which compounds are synthesized in a wave of chemical reaction (Combustion process) over the starting mixture owing to a heat transfer which proceeds layer by layer [61]. Synthesized BNNTs were ready for ion implantation. Now samples were prepared for ion implantation on glass substrates. Different ion doses were applied on different samples to see the effects of ion implantation with the varying dose (in terms of displacements per atom). This chapter covers a brief introduction to the process of synthesis of h-BNNTs and ion implantation processes of nanotubes to get boron carbonitride nanotubes.

2.1 Synthesis of hexagonal multi-walled Boron nitride nanotubes

A very easy and reliable synthesis technique was used to synthesize hexagonal BNNTs in a large quantity. This synthesis process is named as SHS method. Product diameter lies in between 30-200nm. Length of nanotubes was 10µm on average.

DIRECTION
OF
SYNTHESIS
WAVE

PRODUCT OF
REACTION

ZONE OF
SYNTHESIS

MIXTURE OF INITIAL
ELEMENTS
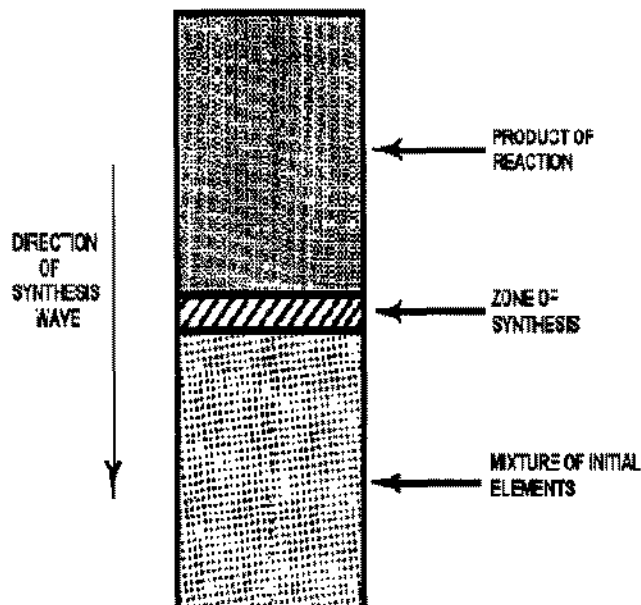
Figure2.1: Diagram of the self propagation high temperature synthesis process [62].

Synthesis process started with preparation of a mixture of 11.90g B_2O_3, 11.60g CaB_6 and 12.20g of Mg. This mixture was prepared by a blender. Time duration of 12min was sufficient to blend the mixture. After that, this mixture was placed in the furnace for 10min under argon atmosphere. Temperature in SHS furnace was maintained to 750°C during the process. Meanwhile SHS reaction occurred in the furnace. After this reaction, a precursor was found in a quantity of 34.80g. This was a porous precursor.

$$3B_2O_3 + 9Mg + 2CaB_6 \rightarrow B_{18}Ca_2(MgO)_9 \tag{2.1}$$
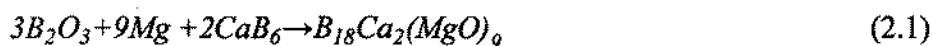
The term $B_{18}Ca_2(MgO)_9$ refers to the product of chemical mixture in the furnace. These chemicals were mixed in a reaction which occurred in the SHS furnace. That reaction started with B_2O_3, Mg, and CaB_6. Precursor was heated by placing it in alumina boat. Temperature was kept at 1150°C at a rate of 6 °C/min. It was kept for 6h in ammonia atmosphere at normal pressure.

23
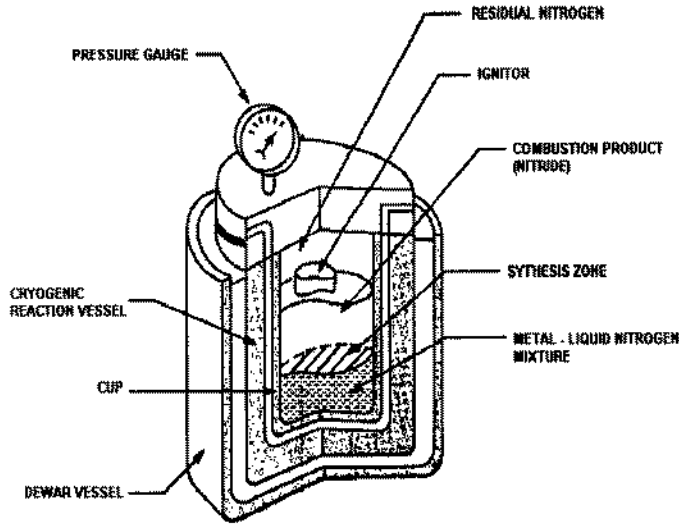
Figure 2.2: Cryogenic reactor used in SHS method [62].

This process was carried out in a tabular furnace. Gas was flowing at a rate of 0.3 – 0.9 L/min along the axis of furnace.

$$B_{18}Ca_2(MgO)_9 + 18NH_3 \rightarrow 18B^* + 18N^* + Ca_2(MgO)_9 + 27H_2 \qquad (2.2)$$
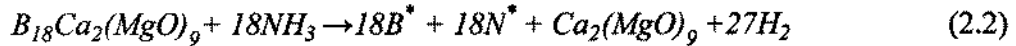
After the reaction occurred, furnace was brought to room temperature for cooling. The crude product was brought out of the furnace. NH_3 reacted with $B_{18}Ca_2(MgO)_9$ and reaction product was obtained in the form of a gas vapor. This gas vapor consisted of hydrogen gas, B* and N* which are highly reactive. Temperature for this reaction was 1150°C. Nanotubes start the growth process at the surface of catalyst droplet. This metal catalyst droplet resides on the surface of MgO. This mechanism is according to VLS growth process. Boron nitride nanotubes began to grow on metal catalysts liquid supported on MgO.

$$x\left(B^* + N^* \right) + Ca_2 (MgO)_9 \rightarrow xBN_{NT} + 2Ca + 9MgO \qquad (2.3)$$

$$(18\text{-}x)\left(B^* + N^* \right) \rightarrow (18\text{-}x)BN_{FL}(x=0 \text{ to } 18) \qquad (2.4)$$
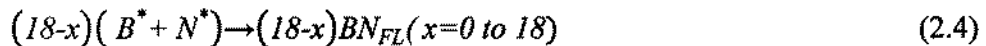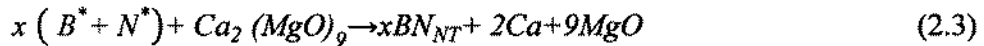
Finally a 5M solution of hydrochloric acid, distilled water and ethanol was prepared to wash the products. After that, product was dried at a temperature of 80°C in vacuum for a time period of 24h. Nanotubes in the form of a grey colored powder (20.25g) were

24

obtained in which Boron in 83.08wt% amount was present. Some flakes were also present in the product. Reason behind the appearance of flakes is the lack of catalyst metal during the vapor-solid phase of growth process. Product selectivity was estimated to be around x/18. For our experiment, parameter x lies in the range of 16 to 18.

Growth process which was used for Boron nitride nanotubes was the base growth mechanism. Liquid droplet of metal has a major contribution in the process of nanotube growth. More over an important feature of VLS growth mechanism is that, the diameters of nanotubes are dependent on the catalyst liquid droplet sizes [62]. Such as small diameters of nanotubes are obtained when liquid droplet size is very small. Similarly large diameters are obtained by large droplets. Thus a certain diameter range could be obtained based on the catalyst droplet sizes. There should be at least one tip initially to grow cylindrical BN structures by base growth mechanism.

Growth rate variations showed that it varies with the microstructure. It smoothly varies with the change in temperature, vapor constitution and the catalyst. Base growth mechanism agrees very well with the product morphology. This mechanism can be explained in the following steps. Firstly, MgO particles act as a base for Ca-B liquid droplet formation. Reaction of liquid droplet occurs with ammonia at a temperature of 1500°C. After the supersaturation stage is arrived by B and N elements, BN nuclei start to precipitate at the surface of liquid droplet. Thus a BN cap is formed with an open top, as illustrated in Figure 2.3.

(a)   (b)
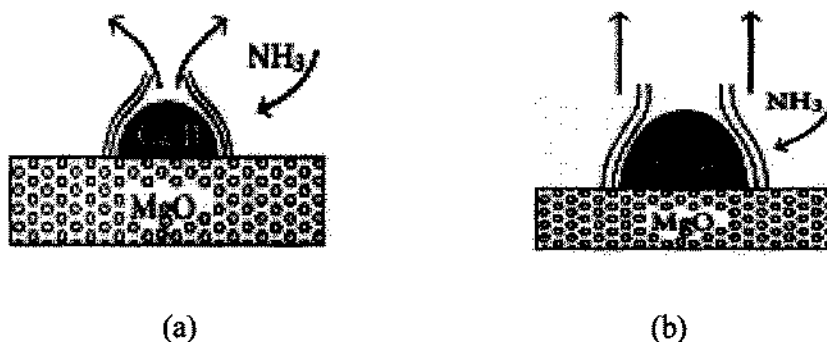
Figure 2.3: Base growth mechanism of BN nanotubes with (a) small radius, (b) large radius [61].

Thirdly, cap gradually grows up into a BN tube, which is a cylindrical structure with an open top. This happens due to availability of free boron and nitrogen species. Since the consumption of both of these atoms, the growth of BNNTs will not stop. Interfacial energy is very small for this type of growth. Liquid-solid interface helps to grow nanotubes with low interfacial energy [63].

(a)   (b)
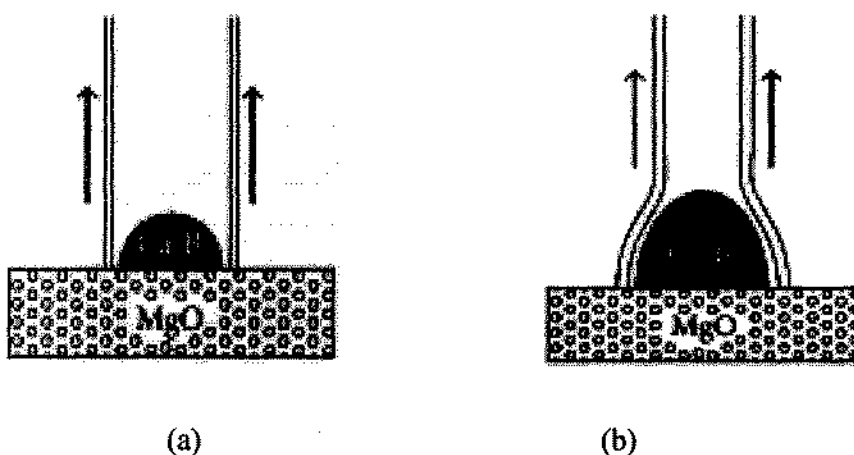
Figure 2.4: Schematic diagram showing the caps grow to form cylindrical nanotubes (a) with small diameters (b) large diameters [61].

2.2 Ion Implantation Process

2.2.1 Sample Preparation:

There are some important steps to prepare samples of as-synthesized BNNTs for ion implantation. These are:

- Cut the glass plates in rectangular shapes of $2 \times 3 cm^2$ sizes with diamond cutter.

- Glass plates are used as substrate of BNNTs for ion implantation process, so they need to be washed. For cleaning, we put them in ethanol and stirred for 15minutes in elmasonic.

A typical glass has the composition given below (table 4)

Table 4 Constituents of Glass [64-65]

Oxide	Weight Percent
Na_2O	13-15
SiO_2	70- 72
CaO	12
Minors	01
Al_2O_3	02

- MWBNNTs were dispersed in ethanol and stirred for 40 minutes to prepare a homogeneous solution.

- Glass substrates were placed on hot plate holding them with tuser. Now drops of the homogeneous solution of BNNTs were dripped one after the other on the glass substrates, to form a film of BNNTs having homogeneous thickness and whose diameter is about 1cm.

- After the deposition of homogeneous film of BNNTs, samples were preserved at room temperature.

After the samples have been prepared, our next goal is to set the parameters for ion irradiation. We have performed calculations with SRIM (Stopping and Range of Ions in Matter) software.

Table 5 Estimated parameters for ion implantation

Ion Element	Thickness of film	Penetration depth	Energy (keV)
Carbon (C)	200nm	170nm	800keV

2.2.2 Ion Implantation:

The samples were irradiated using 5MV Pelletron Tandem accelerator, model 5-UDH, in which source gas (Carbon) was subjected to double boost of accelerations in a single phase. Due to high attractive positive potential, charges are first attracted from ground to high potential end. Electrons are stripped off from the negative ions. Again a boost of acceleration moves these charges to the high potential end of accelerator. During this process a focused beam of C^+ ions was produced. This beam was projected over the target. All the portions of target were homogeneously treated by ion beam. Ion beam current was set at 300nA. In implantation chamber vacuum pressure was maintained to 10^{-6} Torr. Different samples were irradiated with different ion doses. Table 6 summarizes the experimental conditions for ion implantation.

Table 6 Experimental conditions for Ion implantation process

Sample	Ion Type	Dose (Ions/cm^2)	Energy(MeV)
1	Nil	Un-Irradiated	Nil
2	C^+	10^{12}	0.8
3	C^+	10^{13}	0.8
4	C^+	5×10^{14}	0.8

Ion irradiated samples were characterized to confirm carbon implantation in nanotubes. Moreover the effect of dose variation on optical and structural behavior was studied by different characterization techniques.

CHAPTER 3

3 Experimental Techniques

3.1 Ion implantation

Ion implantation was carried out in an electrostatic accelerator. There are two types of electrostatic accelerators.

- Van de Graaff Accelerator
- Pelletron Accelerator

Pelletron accelerators were designed in 1960s. Such an accelerator consisted of charging chains which were a development of the old versions of accelerator. Herb and his coworkers were responsible for this development. Durability of charging chains was superior to charging belts in the old Van de Graaf accelerators. Its stability was more than belts. Issue of dust was resolved by this system of charging chains. There was not any ultimate potential limit and these are successfully used for accelerators having an upper potential limit of 25MV [66].

Pelletron accelerators are of two types

1. Single Ended Accelerator
2. Tandem Accelerator

3.1.1 Tandem Accelerator

In a Tandem accelerator, terminal high voltage is used two times in a sequence. Its purpose is to get output energies with higher orders of magnitudes than the energies available in a single ended accelerator. The source of ion is externally located and negatively charged ions are attracted from ground to the positive terminal due to high

29

attractive positive potential. A striper in the form of a gas canal (argon or nitrogen gas usually) or in the form of a carbon foil of small thickness, is found inside the terminal. Electrons are removed from negative ions by the operation of stripper. Resulting positive charges now experience a second boost from acceleration tube to negative potential (ground) at high energy end of system [67].
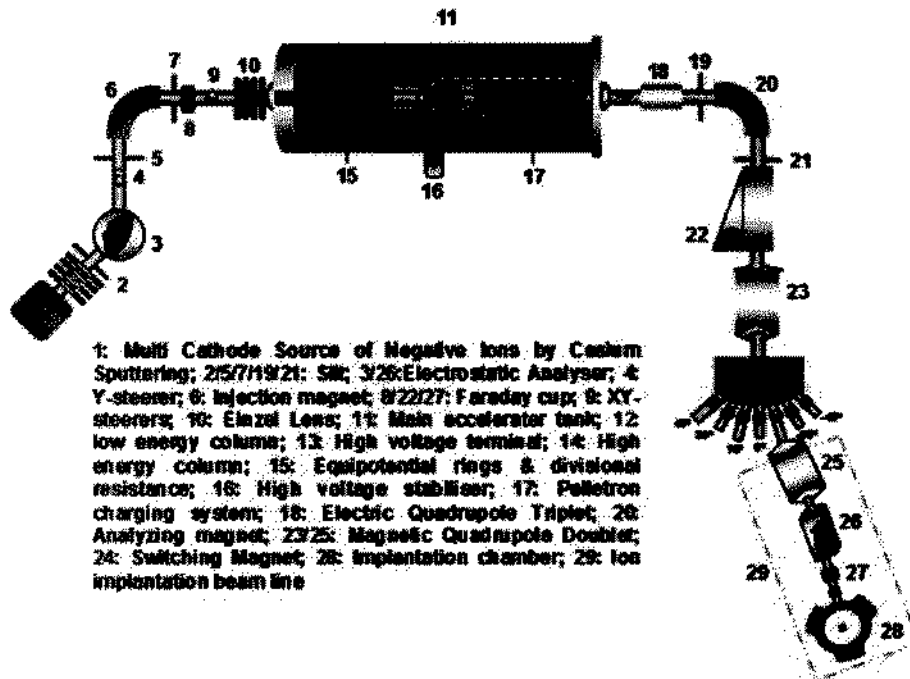
Figure 3.1: Schematic illustration of ion implantation system [67]

3.1.2 Tandem accelerator at National Centre for Physics (NCP):

This research work is carried out at National Centre for Physics by using 5MV Tandem Accelerator, model 5-UDH. 5-UDH Tandem accelerator works under double acceleration. It is an electrostatic accelerator which can deliver ions within the range of 0.8 -30MV. Rated value of the potential is setup after a few minutes of system startup. This electrostatic accelerator is comprised of three major components.

1. Sources of ions
2. Accelerator tank
3. End station

30

Operation:

There are basically two sources of negative ions provided by cesium sputtering (SNICS) and radio frequency (RF). Either of these sources produces a beam of negative ions. Ion beam is extracted and accelerated to energy of 25keV, by the function of extractor. Extractor also measures the beam current and directs the beam into a low energy beam line from Faraday cup to injector magnet. Positive potential generated at the terminal of accelerator tank provides first boost of acceleration to the negative ions. Stripper with Al or N_2 gas strips-off the electrons from negative ions and results in the formation of positive ions. In the acceleration tube, ions gain energy. This energy gain is determined by

$$E = (n+1)V \tag{3.1}$$

V denotes the terminal voltage and n represents the state of positive ions after stripping. Finally, this positive ion beam is directed towards the ion implantation chamber. The beam deflection is achieved by a very large switching electromagnet.
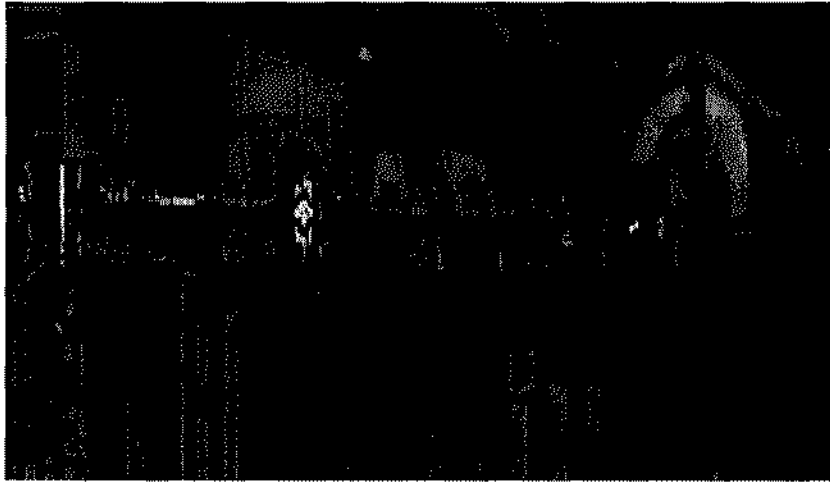
Figure 3.2: 5UDH Pelletron Tandem accelerator at National Centre for Physics [68]

3.2 Characterization Techniques

Sample characterization is an important part of this study. It helps to find out the crystallinity, structure and electronic behavior of the synthesized material.

The synthesized boron nitride nanotubes were characterized by XRD, UV-absorption spectroscopy, HRTEM, SEM, IR spectroscopy and non-Rutherford backscattering spectroscopy in order to determine crystalline structures, electronic behavior, morphological transitions, shapes, dimensions, chemical bonds and elemental contents in ion implanted nanotubes respectively.

3.2.1 Morphological and Micro-structural Investigation

Morphology and microstructure were investigated using Scanning Electron Microscope SEM and Higher Resolution Transmission Electron Microscope (HRTEM).

3.2.1.1 Scanning Electron Microscopy (SEM)

Morphological studies of the products are done with scanning electron microscope. As the name implies, SEM uses electrons for image formation [74]. Scanning electron microscope can provide following types of useful information:

- Morphology and texture
- Crystal structure
- Chemical composition

Principle:

A beam of high energy electrons is focused on a specimen to generate a large variety of signals at the specimen surface. Electrons that are accelerated in a scanning electron microscope carry a large amount of kinetic energy. This energy is utilized to produce various signals by interaction of electrons with the sample. By this interaction following types of signals are received: secondary electrons backscattered diffracted electrons (EBSD), Backscattered electrons, visible light, photons, and heat. Information about morphology and topography of the samples is provided by Secondary electrons [76].

SEM Setup

Electron/Specimen Interactions

When the electron beam strikes the sample, both photon and electron signals are emitted.
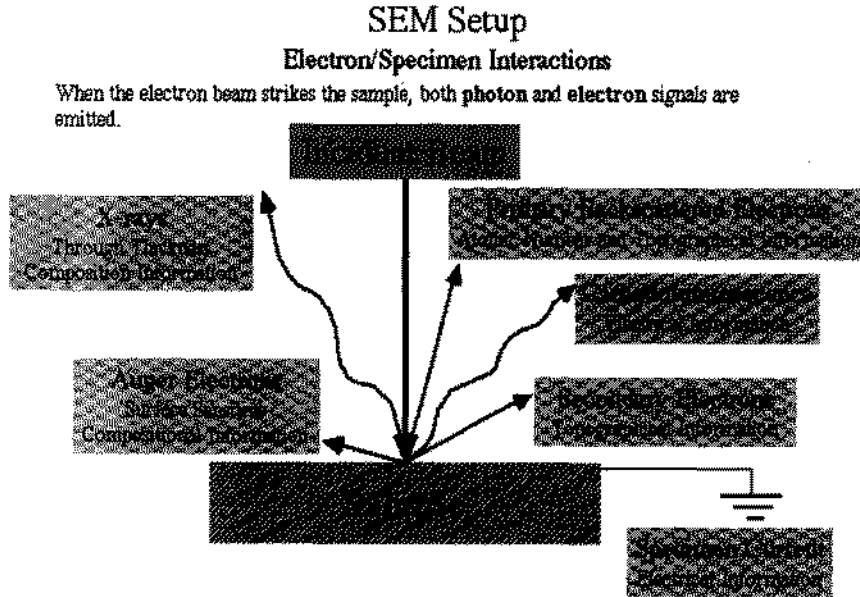
Figure 3.3: Electron beam and specimen interactions [75]

Working:

Electrons are provided by Schottky, thermionic or field emission cathode. Voltage difference between cathode and anode can range between 0.1keV to 50keV. Two or three stage lens system is used to demagnify the smallest cross-section of beam at the gun.
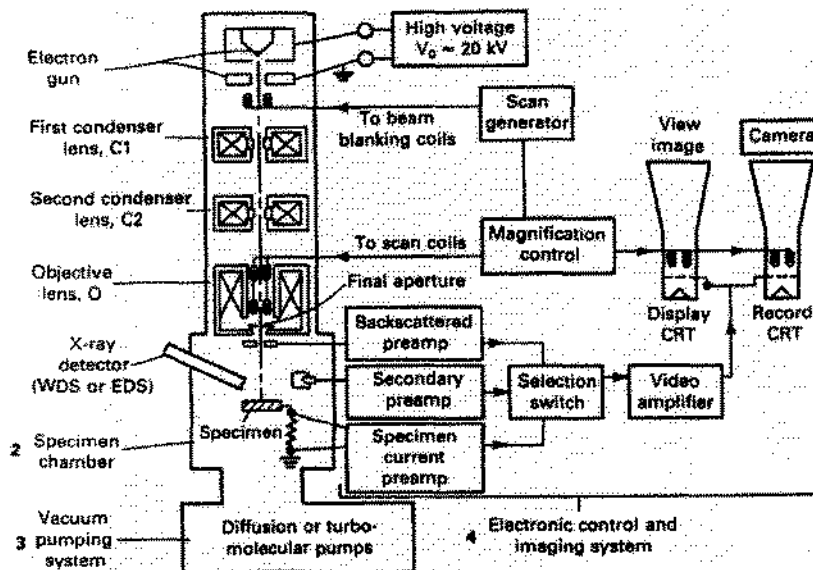
Figure 3.4: Schematic diagram of electron and X-Ray optics of SEM [77]

33

SEM is made up of following essential components:

- Electron gun
- Lenses
- Sample holder
- Detectors for detecting all types of signals
- Display unit

At least one type of detector (usually a secondary electron detector) is most commonly found in all types of SEM. Some microscopes are equipped with additional detection systems [19]. Basically SEMs are of two types (a) Regular SEM (b) Environmental SEM. Conductive samples are needed for analysis in regular SEM, whereas environmental SEM is capable of examining the non-conducting samples as well. Thus in environmental SEM samples are analyzed without any conductive coating. In this research work, BNNTs were examined by using a regular SEM.

Following steps are essentially carried out for sample preparation:

1. Vaporizable materials are removed carefully from the samples, such as water, solvents etc.

2. Samples are firmly mounted.

3. If samples are non-metallic, so they need to be coated by electrically conductive material [76, 77].

Different types of ultra thin conductive coatings are used for non-conductive materials, such as gold, platinum and tungsten. Purpose of coating an electrically conductive material is to avoid the accumulation of charges on the surface during the process of electron irradiation. Coating is also useful to improve image quality, contrast and resolution.

Applications:

SEM is capable of identifying phases of materials. Phase identification depends on crystalline structure and chemical analysis. SEM can examine more than one sample at one time. Images are obtained with high resolution. Sample preparation for SEM analysis

is relatively easier, as conductivity is the only requirement for analysis. Samples sizes from 5microns to 1cm are analyzed in SEM. Magnification of 20 to 30,000 times is possible and spatial resolution of 50 to 100nm is achieved.

3.2.1.2 Higher Resolution Transmission Electron Microscopy (HRTEM)

Investigation of crystallographic structure is now possible with higher precision by means of an imaging tool. HRTEM is a modified form of Transmission Electron Microscope. Defects and crystallographic details are made visible with this tool in the form of a two dimensional image. Atoms and crystal structures can be individually viewed. Image is formed by phase-contrast. In Transmission Electron Microscope, theory of phase-contrast helps to achieve a higher resolution (less than one angstrom). Thus atoms can be distinguished from each other on the basis of their different index of refraction. As different materials have different refractive indices, so bending and passage of electron beam through these materials is influenced by them. Due to this effect, some waves are not in phase with others. Thus an image is formed as a contrast of dark and bright areas [69].

Principle:

When electron beam is allowed to fall on the sample surface, interaction of each individual electron with the matter is observed.
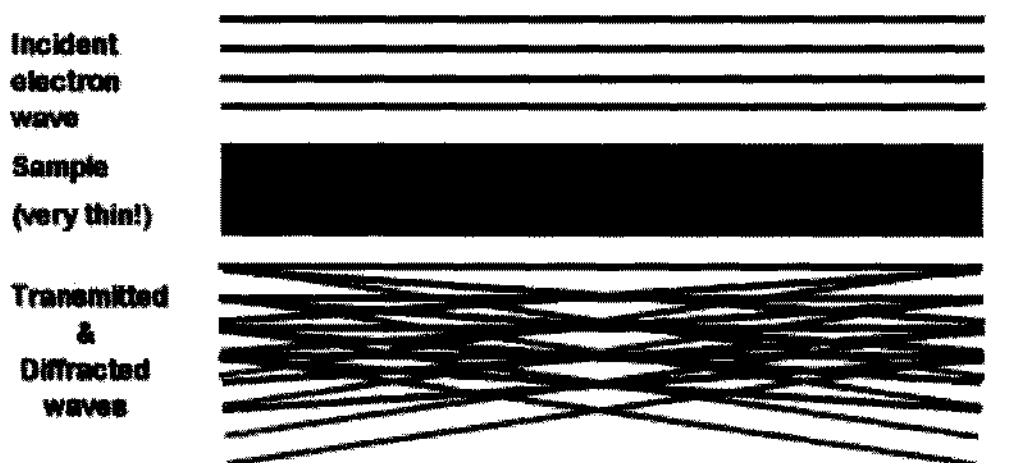
Figure 3.5: Phase contrast for diffracted and transmitted electron waves [70].

35

Before the electron beam enters the sample, it can be thought of as a plane wave. But the moment it penetrates inside the material, atomic cores offer a positive attractive potential. Channels of atomic columns also offer attractive potentials to the incident electron beam. Electron wave passing through different atomic columns interacts and Bragg's diffraction occurs. When electron beam exits from the sample, it is not only the plane wave but a multitude of beams diffracted from atomic columns superposes with plane wave. This exit electron wave is passed through the imaging section of HRTEM where interference and phase change further proceed due to imaging wave in the plane of image (CCD or photo plate) [71]. Image is formed by interference of diffracted and transmitted waves, because different amount of distance is covered by both types of waves. Solution of Schrodinger equation is different for each diffracted electron beam. Image formation is accomplished in the following two steps:

1. Diffracted waves have phase difference which we need to calculate. An overlap of the interference pattern due to these phase differences helps to form image.
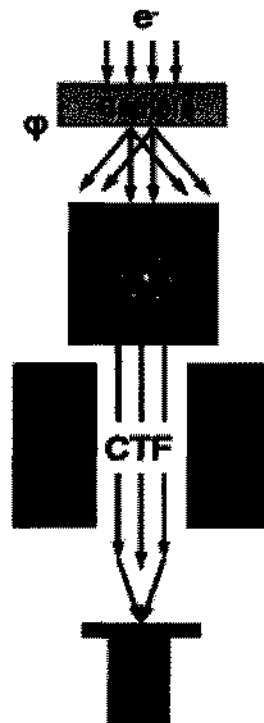
Figure 3.6: Reconstruction of exit ray for image formation in HRTEM [72,73].

2. Since the exit wave and image wave have a non linear relationship thus aberrations are always present in the image contrast of HRTEM, which strongly depends on defocus Δf, diffraction vector, coefficient of spherical aberration C_s and wavelength of electron beam. These aberrations always cause a phase shift of diffracted waves by objective lens. A function that limits the aberrations and apertures in the lenses is known as Contrast Transfer Function (CTF).

Applications:

1) HRTEM offers a resolution less than 1nm. Thus nanoscale studies of materials require this imaging tool.

2) Dislocations, interfaces and defects can be directly observed at atomic scale.

3.3 Structural Investigation

3.3.1 X-Ray Diffraction (XRD) Technique

In the beginning, it was considered that the solids are made up of periodically arranged atoms but there was not any experimental evidence of this idea. After the discovery of x-rays, it was possible to probe the materials for their phase and structure determination [78].
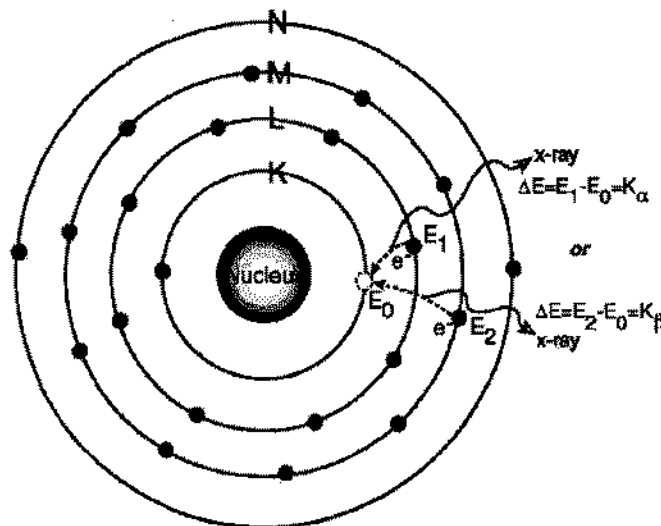
Figure 3.7: Emission of X-rays from atoms [80]

Diffraction patterns are obtained by X-Rays because wavelength of X-Rays is comparable to the spacing d between atomic planes [79]. Figure 3.7 represents the emission of X-rays by K-shell transitions. Only those X-rays are used for diffraction analysis, which are emitted due to K shell transitions because of their smaller wavelength as compared to those emitted by L or M-Shell transitions [81].

X-Ray Diffraction provides essential information for identification of a crystal. Moreover, understanding of unit cell dimensions is developed by diffraction patterns obtained by this technique. This is based on constructive interference of X-Rays diffracted from various crystal planes. When conditions of Bragg's law are satisfied, then conditions for constructive interference are met [81, 84].

An English physicist, Lawrence Bragg proposed the idea of wave diffraction through crystal planes. He formulated a law, which describes a relationship between the incoming radiation, diffraction angle and lattice spacing in a crystalline material.

$$n\lambda = 2d\sin\theta \qquad (3.2)$$
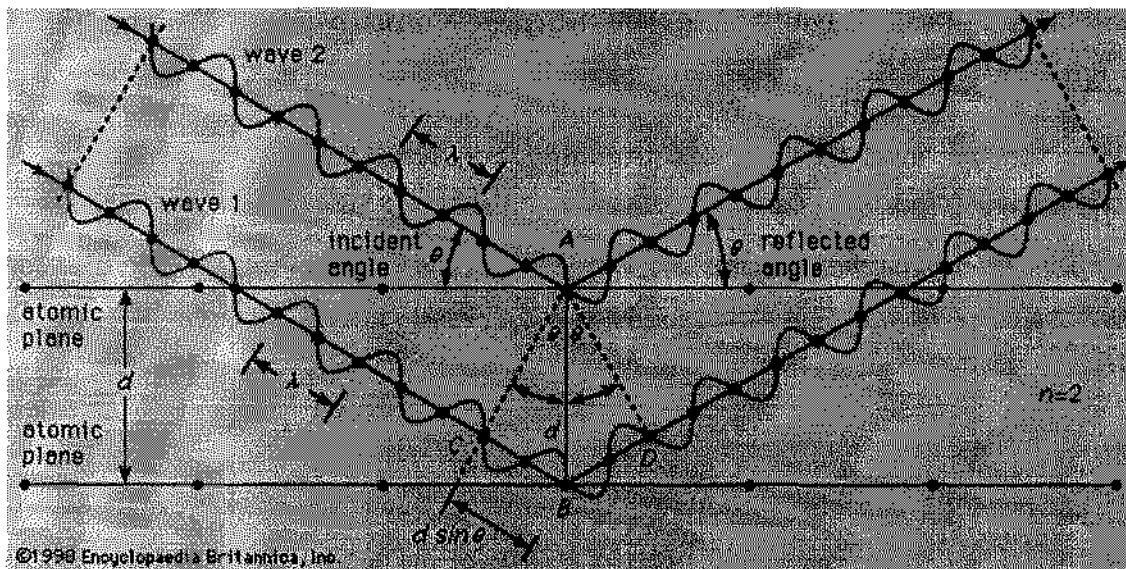
Figure 3.8: X-rays reflections from two atomic planes in solids [82]

Here n (being an integer) gives the order of diffraction. Usually any order of diffraction is considered as first order (i.e. $n = 1$) from planes spaced at $1/n$ distance apart from

previous one. Since for any values of Bragg's angle, $Sin\theta$ cannot exceed unity so we may write a condition for diffraction as, $Sin\theta = (\lambda/2d) < 1$; $\lambda < 2d$. This employs that x-rays used for diffraction must have a wavelength always less than atomic spacing (i.e. 2d). Following types of information can be obtained by X-Ray diffraction technique [83-86].

1. Crystalline and amorphous materials can be differentiated. As sharp diffraction peaks belong to crystalline materials, which show that atoms are arranged periodically along various planes. In amorphous materials, no sharp peaks are observed. Only a few broad peaks appear in the diffraction pattern.

2. Crystal structure (axes, positions of atoms, shape and size of unit cell) can be determined.

3. Electronic distribution in the unit cell as well as in atoms can be determined.

4. Single crystal's orientation can be determined by X-Ray diffraction studies.

5. Grain sizes can be determined. It is also possible to determine texture of such materials. Grain size is calculated from full width at half maximum of diffracted lines. Following formula is used for this calculation.

$$t = \frac{0.9\lambda}{B \cos \theta_B} \tag{3.3}$$

Where λ, t, B and θ_B are the wavelength of incident beam, particle/grain size, full width at half maximum(FWHM) and exact Bragg angle. We can determine (FWHM) by the following formula

$$B = \frac{1}{2} (2\theta_1 - 2\theta_2) \tag{3.4}$$

Here θ_1 and θ_2 are values of Bragg angles at two different peak positions.

6. Relative proportions and crystalline phases can be identified by XRD. Density of the unit cell is given by the formula

$$\rho = \frac{\Sigma A / N_A}{V} \tag{3.5}$$

Here ΣA represents atomic weight of all the atoms present in unit cell, unit cell volume is denoted by V and N_A represents Avogadro's number.

7. Phase diagrams can be determined; moreover limits of solubility of solids can be measured by XRD.

8. Strain measurements are also possible with XRD studies.

9. Imperfections and randomness of crystal structures are also measured with XRD technique.

10. Functions of radial distribution can be estimated for non-crystalline solid and liquid materials.

Moreover qualitative and quantitative analysis based on chemical composition is possible.
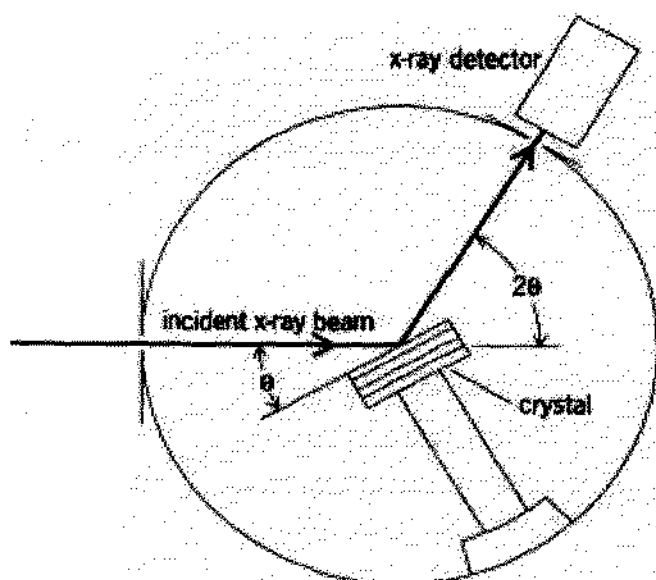
Figure 3.9: Schematic diagram of X-ray diffraction [84-86]

Schematic illustration of an X-Ray diffraction tool is given in Figure 3.9. X-Ray diffractometer are made up of three basic components:

a. X-Ray tube which emits incident X-Rays.

b. Sample holder

c. Detector for X-Rays detection.

The resulting diffraction patterns are interpreted with the help of crystallography software. Angular positions of sharp diffraction peaks help to determine geometry and size of unit cell. Arrangement of atoms is related to intensities of diffraction peaks.

3.4 Composition Spectroscopy

3.4.1 Non-Rutherford Backscattering Spectroscopy (NRBS)

An efficient analytical tool for elemental characterization of various materials is "Ion Backscattering Spectrometry". Backscattering spectrometry is a versatile technique. Rutherford backscattering is one of the ion backscattering studies, which is very straightforward technique. It is possible to determine the composition and thickness of thin films (<4000 Å). One of the lately explored ideas of this field is the use of backscattering technique to determine the composition of superconductor oxides. With this technique we can analyze the lattice mismatch of epitaxial layers. Moreover morphology of thin films and surface clustering can be studied. When two bare nuclei interact with each other, then according to Rutherford backscattering model a repulsive potential $V \sim q/r$ is established [87- 90].

Backscattering spectroscopy gives us the following useful information:

- Mass resolution of materials
- Depth distribution of energy in materials
- Elements in the sample composition

An apparatus consisting of the following three components is used for backscattering studies of thin layers of solids:

1. Helium ions source.

2. Accelerator to provide energy to ions.

3. Detector/ energy analyzer.
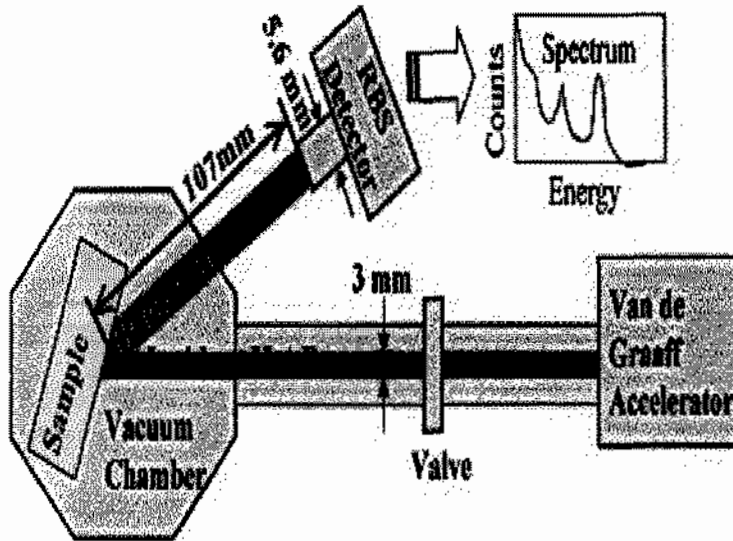
Figure 3.10: Schematic diagram of Backscattering Spectroscopy [88]

Basic analytical characteristics of ion backscattering, the capability of mass, depth and quantitative analysis, are based on the energy exchange between the elastically colliding particles, the slowing down of the ion in target material, and the probability of the elastic collision reaction. Thus collision phenomena are theoretically treated in terms of the collision kinematics, stopping power, and the scattering cross section, respectively.
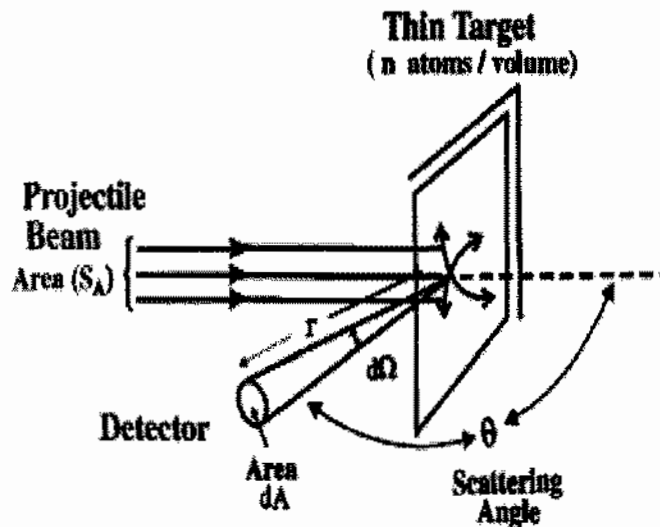
Figure 3.11: Schematic illustration of scattering cross section in terms of θ (Scattering angle) and $d\Omega$ (solid angle) [91].

Whenever we are interested to calculate the scattering cross-section, we need to have sufficient information about the nature of interaction between target and projectile. Required information for calculation of scattering cross-section includes initial and final energy states, angle of scatter and spin etc. Total solid angle can be integrated to calculate the Rutherford scattering cross section, as under

$$\sigma_R(E,\theta) = \frac{(Z_1 Z_2 e^2)^2}{(8\pi\varepsilon_\circ E)^2} \frac{1}{\sin^4\theta} \frac{[M_2\cos\theta + (M_2^2 - M_1^2\sin^2\theta)^{1/2}]^2}{M_2 \times (M_2^2 - M_1^2\sin^2\theta)^{1/2}} \tag{3.6}$$

Note that σ_R is proportional to $Z_1^2 Z_2^2/E^2$, therefore sensitivity increases with increasing atomic numbers Z_1 and Z_2 and decreasing energy [89, 91].

Non- Rutherford backscattering spectroscopy (NRBS) is useful for the detection of light elements. In Rutherford Backscattering spectroscopy (RBS) nuclear charges are assumed to be completely unscreened. But sometimes interaction is slightly different. When the point charges collide in such a way that their collision diameter becomes very small and it is closer to the value of sum of radii of target and projectile. In this case, nuclear forces lead to such interactions for which scattering cross sections are not the same as Rutherford cross sections. Mostly this behavior is observed in the target materials with low atomic numbers, because for them coulomb barrier is very small. In this case scattering cross section is many orders of magnitude greater than Rutherford scattering cross section. This is nuclear resonance scattering which is very useful to detect low Z elements [89]

In case of non-RBS , nuclear forces between target and projectile are very important. Non-Rutherford cross sections are observed when incident energies E and scattering angles θ are high and atomic number Z of target is low. When energy is very high, projectile nucleus approaches the target at a distance of closest approach which is comparable to the nuclear dimensions. Thus a deviation from Rutherford scattering cross section is observed due to which short range nuclear forces become important for scattering phenomena. In case of inelastic scattering, energy is not simply KE_0 for scattering particles. Thus energy, scattering angle and combination of target and projectile determines the scattering cross section [91].

During RBS measurements, a region of energy is observed in which resonance phenomena occurs. But sometimes an enhanced or smooth variation in the resonance energy region is observed. Such variant cross sections, which do not follow Rutherford phenomena, are known as non-Rutherford cross sections. Non-Rutherford cross sections are several orders of magnitude greater for lighter elements as compared to Rutherford values. At a backscattering angle of $165°$ between the energy range (8.0-11.7 MeV) , α - particles were used to detect carbon. A proton beam of 2.4MeV energy is found to be very sensitive for carbon, oxygen and nitrogen. α-particles beam with (3.06MeV) energy is very sensitive for oxygen [90,91].

Non-Rutherford cross sections, for scattering angles in the range of $160°$ to $180°$ are observed for the energy values:

For protons: $E_{Lab}(MeV) = 0.12Z_2 - 0.5$

For α-particles: $E_{Lab}(MeV) = 0.25Z_2 + 0.4$

3.5 Vibration Spectroscopy

Bonding states and compositional profile is analyzed with the help of vibration spectroscopy. Figure 3.12 summarizes the vibrations related to each part of the electromagnetic spectrum.

Wavelength (m)	10^{-10} 10^{-9} 10^{-8} 10^{-7} 10^{-6} 10^{-5} 10^{-4} 10^{-3} 10^{-2} 10^{-1} 10^{0} 10^{1} 10^{2} 10^{3}
Frequency (MHz)	3×10^{10} $\quad$ 3×10^{8} $\quad$ 3×10^{6} $\quad$ 3×10^{4} $\quad$ 3×10^{2} $\quad$ 3
Type of radiation	X-rays Ultra Visible Infrared Microwaves Radio γ-rays violet waves
Energy levels of appropriate transitions	Atomic electronic transitions Atomic and molecular electronic transitions Molecular vibrations Molecular rotations Nuclear magnetic energy levels

Decreasing energy ⟶
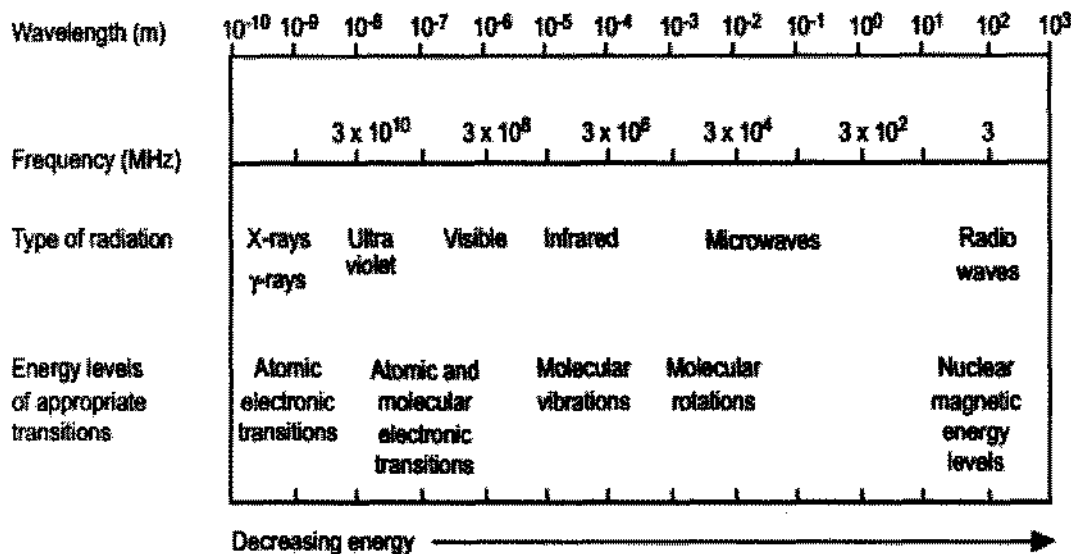
Figure 3.12: Regions of the electromagnetic spectrum [33]

3.5.1 Infrared Spectroscopy (IR)

Chemical bonds in a material are identified by infrared Spectroscopy. Functional groups in the synthesized material can also be identified by this technique.

There are three main catagories of infrared spectrum:

1) Near Infrared ($14285cm^{-1}$-$4000cm^{-1}$)

2) Mid Infrared ($4000cm^{-1}$-$400cm^{-1}$)

3) Far Infrared ($400cm^{-1}$-$0cm^{-1}$)

An Infrared beam in the mid infrared range of spectrum is used to characterize the samples. When this beam interacts with the sample, it is partially transmitted and partially absorbed. A comparison is made between the radiations passed through reference cell with those passed through the sample [92].

Absorption of IR beam in the molecules results in periodic vibrations of molecules. Radiation absorption in the sample depends on the structure and strength of bonds. Atomic masses also affect the absorption of IR beam in matter. Lattice vibrations are induced due to absorption of radiation, which are also known as phonon motion.

Absorption peaks in the IR spectra indicate the frequencies with which bonds between the atoms vibrate. Because each material is made up of different types of atoms, thus IR spectrum of different types of materials can never be same due to their different bonding nature and associated polarizibilities [92].
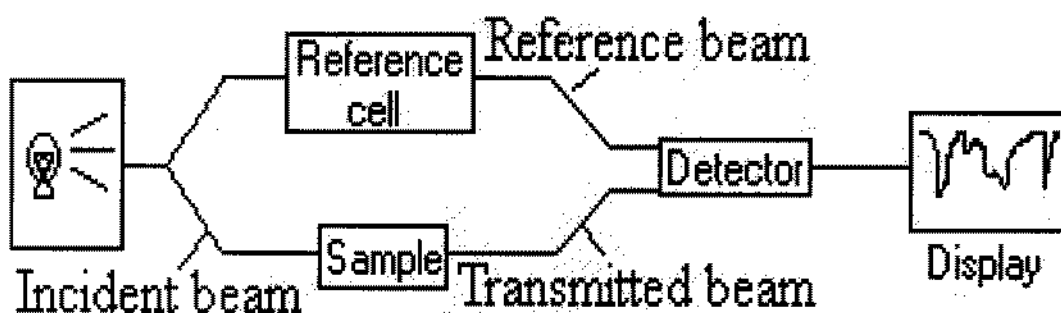
Figure 3.13: Apparatus for IR spectroscopy [94]

Attenuated Total Reflection (ATR):

Attenuated total reflection (ATR) is a type of Infrared spectroscopy that is being used for a wide range of samples. Solid as well as liquid samples can be efficiently analyzed. Moreover there is no issue of spectral reproducibility and sample preparation. This accessory works on the following principle. When IR beam interacts with the sample, it is totally internally reflected in the sample [93].

The useful information provided by IR spectroscopy is as under:

1. Unknown materials can be identified.

2. When the sample is in the form of a mixture, we can judge the quality of mixture components.

3. Qualitative analysis of samples can be made.

Working:

Sample is kept in touch with an optically dense crystal, whose refractive index "n" lies between 2.38 to 4.01 at $2000cm^{-1}$. Sample must have a low refractive index as compared to that of the crystal. But luckily a wide range of liquids and solids have very small value of refractive index. Beam is allowed to fall on the crystal surface at some specific angle. Beam enters in the crystal and is totally internally reflected.
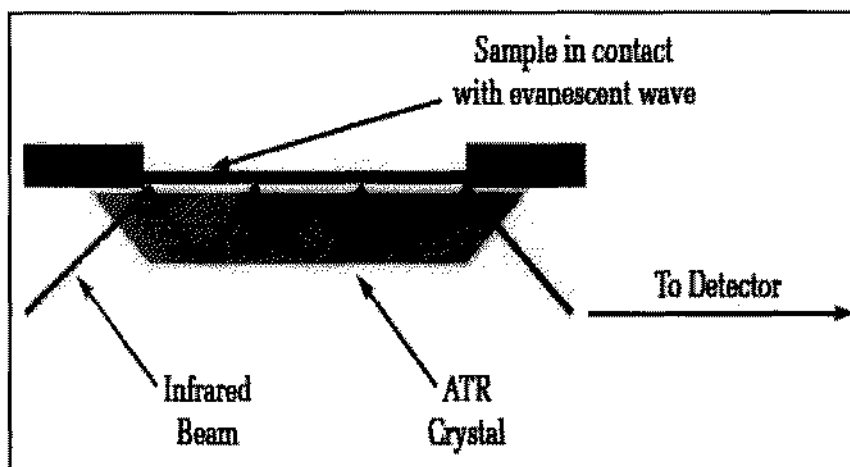
Figure 3.14: A multiple reflection ATR system [93].

According to thickness and length of crystal, usually beam is reflected five to ten times in the crystal. As a result of total internal reflection, a wave is created on the crystal surface. This wave protrudes into the sample kept in touch with the crystal surface. This is an evanescent wave which resides on the surface of crystal just as an IR bubble. It is necessary to ensure a good contact of crystal surface and the sample; because wave can extend into the sample up to a few micrometers typically $(0.5\text{-}5\mu m)$. When the wave experiences multiple reflections in the crystal, a part of its energy is absorbed by sample. Due to this absorption, IR beam attenuates. These evanescent waves pass their attenuated energy to infrared beam, which leaves the crystal and enters into a detector. Detector measures the changes in IR beam after passing through sample and crystal. Fourier transform infrared spectroscopy with ATR accessory is provided with the following characteristics:

1. A large variety of liquid and solid samples can be analyzed.

47

2. Data of excellent quality can be achieved with IR spectroscopy and Spectral variations are minimum

3. Sample preparation is not difficult and reproducibility is improved.

3.5.2 Raman Spectroscopy

Raman spectroscopy is the measure of inelastic scatterings of light. When a beam of monochromatic light is incident on a sample, photons are scattered from the specimen surface. Now if we carefully observe the frequencies of scattered light, we see that frequency of incident photons and that of scattered photons is not the same. Thus upon interaction, a change in frequency is observed. Whenever a beam of light from a laser source is incident on some material, it is absorbed and reemitted. During this process frequency is shifted up or down as compared to the frequency of incident monochromatic light. This phenomenon is named as Raman effect. Frequency shift provides helps to understand the rotational, vibrational and all other types of molecular transitions [95].

Principle:

Polarizibility of the molecules α determines the deformations of molecules in electric field E under the action of incident monochromatic light. This is the basis of Raman effect. Beam of light emitted from a laser source is an electromagnetic wave with E as its electrical vector. When this radiation interacts with the matter, a dipole moment $P = \alpha E$ is induced which causes molecular deformations. These molecular deformations are periodic and stimulate periodic vibrations of the molecules with a definite frequency v_m [96].

Difference in energy of incident and scattered photon causes a frequency shift known as Raman shift. Thus an incident beam of monochromatic light having frequency v_o interacts with matter and molecules are transformed into oscillating electric dipoles.

Radiations which are emitted from oscillating electric dipoles can have frequencies of three different types (Figure 3.15):

1. When a molecule is not Raman active, its interaction with the photon is elastic, named as Rayleigh scattering. In this type of interaction, molecules absorb photons

48

with frequency v_o and move from basic state of vibration to excited states. These excited molecules return back to their ground state and emit light having frequency v_o , which is the same as the frequency of absorbed photons [97].
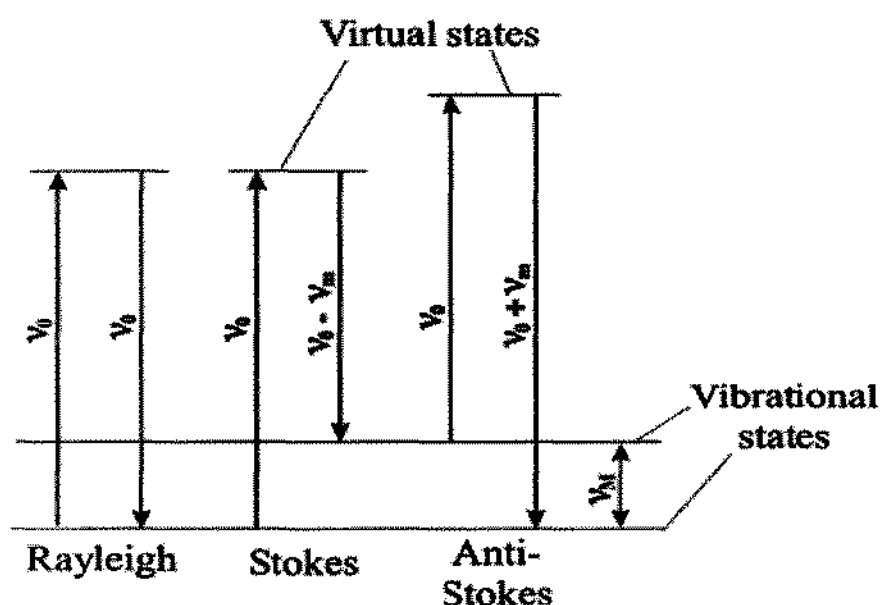
Figure 3.15: Raman Transitional Scheme [97]

2. A Raman-active molecule interacts with light in two different ways.

   (a) Molecule absorbs a photon at the instant when it is in the basic state of vibration. At that time, frequency of absorbed photon is v_o. Photon is released with a frequency $v_o - v_m$. This is due to partial transfer of photon's energy to Raman-active modes, so a change in frequency is observed. The frequency $v_o - v_m$ is known as "Stokes" or "Stokes Frequency".

   (b) Molecule is in the excited state when a photon interacts with it having frequency v_o , it is absorbed. When molecule reemits the photon to return back to the basic state of vibration, it releases the photon with the excessive amount of energy. Thus photon is emitted with frequency greater than that of absorbed photon. The frequency $v_o + v_m$ is known as anti-stokes or anti-stokes frequency [96].

Schematic diagram of spectrometer:
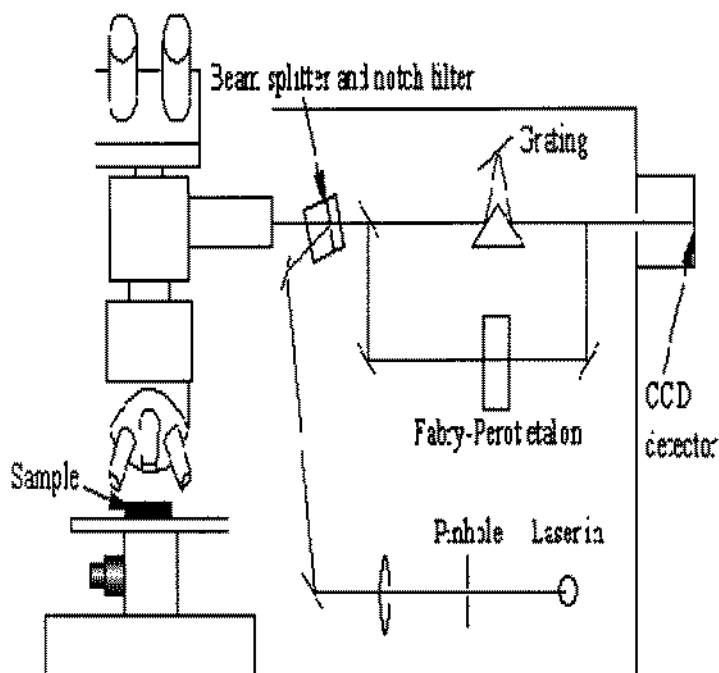
Figure 3.16: Schematic diagram of Raman spectrometer [98]

Mostly a photon that interacts with the sample, it is elastically scattered, thus it exhibits Rayleigh scattering. Energy shift from frequency of incident light is observed only 10^{-5}% of the intensity incident light. Thus when electromagnetic waves interact with vibrational states of molecules in the matter, frequency shift is rarely observed. That's why Raman signal is of very low intensity. Physicists are constantly trying to find the ways to improve signal strength. A plot between the frequency and intensity of light (which is subjected to frequency shift) gives Raman spectra of a material [99].

Characteristics of Raman spectroscopy are as under [100]:

1. It is more efficient than near-infrared and mid-infrared spectroscopy for finger printing and probing the molecular symmetries.

2. It does not require fancy sample preparation, sample holders of glass are used which are not costly.

3. Raman signal is usually very weak and virtually anti-stokes lines are used due to get stronger signal intensity.

4. Raman modes provide information about chemical structure due to availability of fundamental modes.

5. For the characterization of inorganic and organic samples, spectral range below 400cm^{-1} is reached.

6. Raman spectrum is clean as compared to other electromagnetic spectra. Narrower Raman bands are observed while combination and overtone bands are weaker.

7. Raman spectra of all types of samples can be recorded, thus it is successful for liquids, solids and gaseous substances.

8. It is a non-destructive and straight forward technique.

3.6 Optical Studies

Optical studies were performed to study band gap of nanotubes, by using a UV-Spectrophotometer.

3.6.1 Absorption spectroscopy by UV- Spectrophotometer

Visible or Ultravoilet light is absorbed by molecules such that beam is attenuated as well as absorbed rapidly. Hence absorbance is found to be proportional to quantity of attenuation. Radiation is absorbed for that particular value of frequency for which the difference in energies between two quantum mechanical states of molecules matches with each other. According to Beer's Law, absorbance increases with an increase in path length and quantity of species that absorb light.

Mathematically,

$$A = ebc \tag{3.7}$$

Here A stands for absorbance, b denotes path length, c is concentration of absorbing molecules and e is proportionality constant, named as absorbtivity. Visible light contains a wide range of wavelengths, molecules respond to these wavelengths quite differently. A molecule can have various structural groups in itself and these structural groups stimulate different absorption bands in the spectra [101].

Table 7 Wavelength, frequency and energy used for UV-absorption spectroscopy [102].

Wavelength (λ) (nm)	Frequency (υ) (Hz)	Energy (E) (kJmol^{-1})
900	3.33×10^{14}	137.5(Infrared)
700	4.29×10^{14}	171.2(Red light)
400	7.50×10^{14}	299.3(Blue light)
190	1.58×10^{15}	630.5 (Ultravoilet)

Wavelength, energy and frequency are interrelated by:

$$c = \upsilon\lambda \qquad (3.8)$$

Similarly energy is given by,

$$E = h\upsilon$$

(3.9)

Where,

c=speed of light $(3.0 \times 10^{8} ms^{-1})$

λ=wavelength(m),

h= Planck's constant $(6.63 \times 10^{-34} Js^{-1})$

υ=frequency (Hz)

The origin of the absorptions

Whenever a beam of light is absorbed by a molecule, electrons in the outer most shell of the atoms are excited to higher energy states. Whether the light is visible or ultravoilet, electrons absorb energy and move from ground to excited states. Atoms move in the molecules with respect to other atoms, they do not remain stationary. Their movement

may be in the form of vibration or rotation. Discrete energy states are induced due to such vibration or rotation, these energy states lie above each other [103].
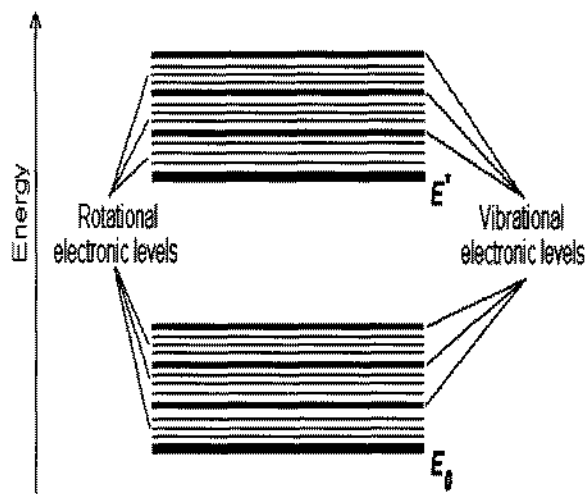
Figure 3.17: Discrete energy levels corresponding to rotations and vibrations [102]

There are three types of electron shells in which valence electrons reside:

1. Orbital with single bond called σ bonding orbital.
2. Orbital in double or triple bonding state i.e. as π bonding orbital.
3. Orbital having lone pair of electrons i.e non-bonding orbital.
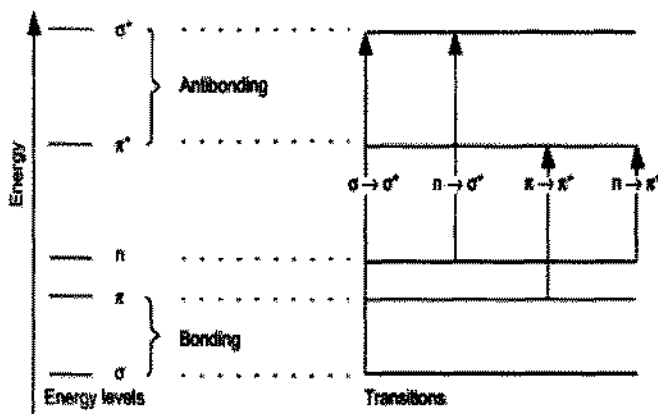
Figure 3.18: Electron transitions in ultraviolet/visible spectroscopy [103]

Orbital having a single bond is in a low energy state as compared to that having double or triple bonds. Moreover energy of non-bonding orbital is always less than sigma bonding orbital. As an electromagnetic radiation interacts with matter, electronic transitions occur as a result of absorption of radiation. Transitions from above mentioned orbitals are directed towards anti-bonding orbital, π^* or σ^*.

Working:

In a typical spectrophotometer, a square shaped sample holder carries a sample from which an electromagnetic radiation passes. This sample holder is typically 1cm wide. Sample is subjected to electromagnetic radiation for 30 seconds. These electromagnetic waves belong to the whole ultraviolet range of spectrum. A reference cell which contains a solvent is simultaneously subjected to the radiation of same intensity and frequency. Radiations that are transmitted from both, the sample and the reference cell are detected by photocell.
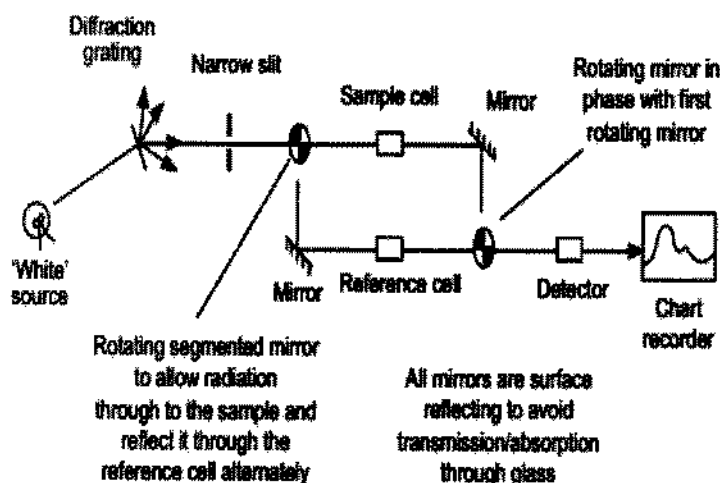
Figure 3.19: Diagram showing how the ultraviolet/visible spectrometer works [101]

Then spectrometer makes comparison between intensities of radiations passing through both objects. Absorption spectrum is finally compiled by a computerized system. Modern spectrometers can simultaneously monitor the radiation chart [103].

CHAPTER 4

4   Results and Discussion

In this research work, 0.8MeV C^+ ions have been successfully implanted in the hexagonal multi-walled Boron nitride nanotubes (h-MWBNNTs) at different ion doses. The samples were irradiated using 5MV Pelletron Tandem accelerator, model 5-UDH in which source gas (Carbon) was subjected to double boost of accelerations in a single phase. Due to high attractive positive potential, charges are first attracted from ground to high potential end. Electrons are stripped off from the negative ions. Again a boost of acceleration moves these charges to the high potential end of accelerator. During this process a focused beam of C^+ ions was produced. This beam was projected over the target. All the portions of target were homogeneously treated by ion beam. Ion beam current was set at 300nA. Vacuum pressure of 10^6 Torr was maintained in the implantation chamber. Different samples were irradiated with different ion doses.

4.1 Morphological and Micro-structural Investigation

4.1.1 Scanning Electron Microscopy

Images of Scanning Electron Microscope (SEM) of nanotubes were taken at different resolutions with electron beam energy of 20kV. SEM images of h-MWBNNTs before ion irradiation at a resolution of 1μm are given in Figure 4.1(a) and 4.1(b).

Figure 4.1: (a) and (b) SEM images of h-BNNTs before ion implantation at a resolution of 1μm.

55

After Irradiation at a dose of 5×10^{14} ions.cm^{-2} nanotube junctions are observed. Two SEM images Figure 4.2(a) and 4.2(b) were taken at a resolution of 2µm and 1µm respectively. Irradiation causes defects and junctions are formed. A strong collision cascade effect starts due to interaction of ion beam with the nanotubes. Neighboring walls of multiwalled cylindrical structures join together. This happens due to interaction of walls and covalent bond formation between the adjacent atomic layers [104-106].
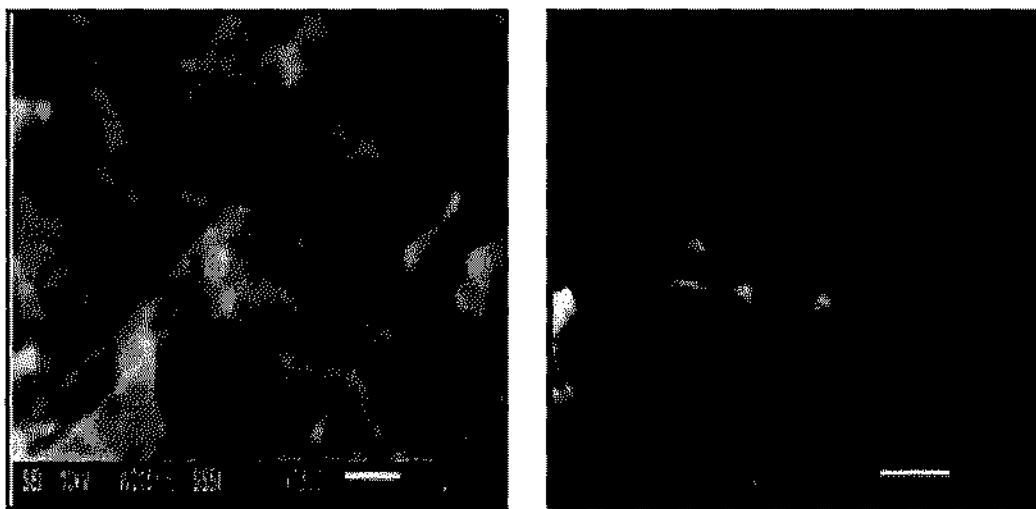
Figure 4.2: (a) resolution of 2µm and (b) resolution of 1µm showing that BNNTs form junctions after ion irradiation.

4.1.2 Higher Resolution Transmission Electron Microscopy (HRTEM)

Higher resolution transmission electron microscope (HRTEM) is used to observe structural and morphological changes in Boron Nitride nanotubes. Four different samples were prepared on a copper grid for TEM analysis. Figure 4.3 is showing HRTEM image of un-irradiated h-MWBNNTs, this image is taken at a resolution of 10nm. Interlayer spacing as mentioned in the image is 0.34nm which confirms the structure of hexagonal boron nitride nanotube [107].
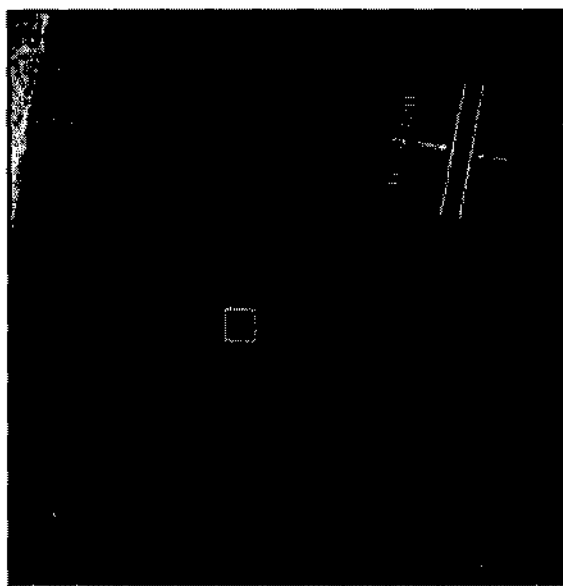
Figure 4.3: HRTEM image of h-BNNT taken with a resolution of 10nm.

When Carbon ion implanted nanotubes were observed in HRTEM, some structural changes were observed. With a carbon ion in a quantity of 10^{12} ions.cm^{-2}, morphological or structural changes were not very apparent. A little bit amorphization is observed on the outer layers of multiwalled nanotubes as in Figure 4.4. Ion irradiation of nanotubes under ion dose of 10^{13} ions.cm^{-2} and 5×10^{14} ions.cm^{-2} gives amorphous nanotubes (Figure 4.5a). These are ion implanted boron nitride nanotubes or boron carbonitride nanotubes, whose outer layers are amorphous and holes are also observed on the surfaces (Figure 4.5b). Amorphization is due to defect formation in bulk. These defects appear when carbon ions interact with h-BN lattice and impart their energy to nanotubes [108].
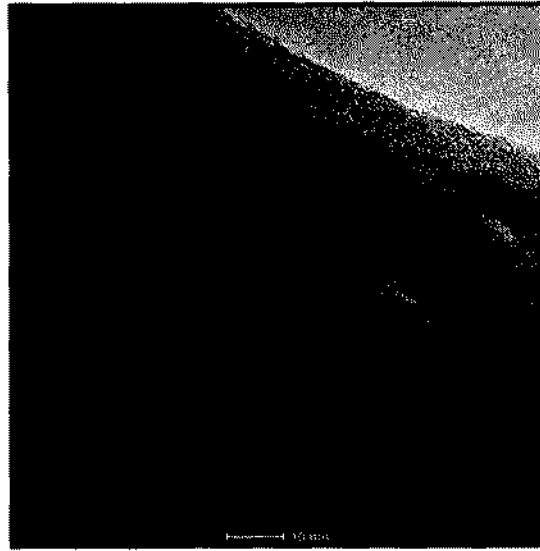
Figure 4.4: HRTEM image of h-MWBNNT at ion dose of 10^{12} ions.cm^{-2}
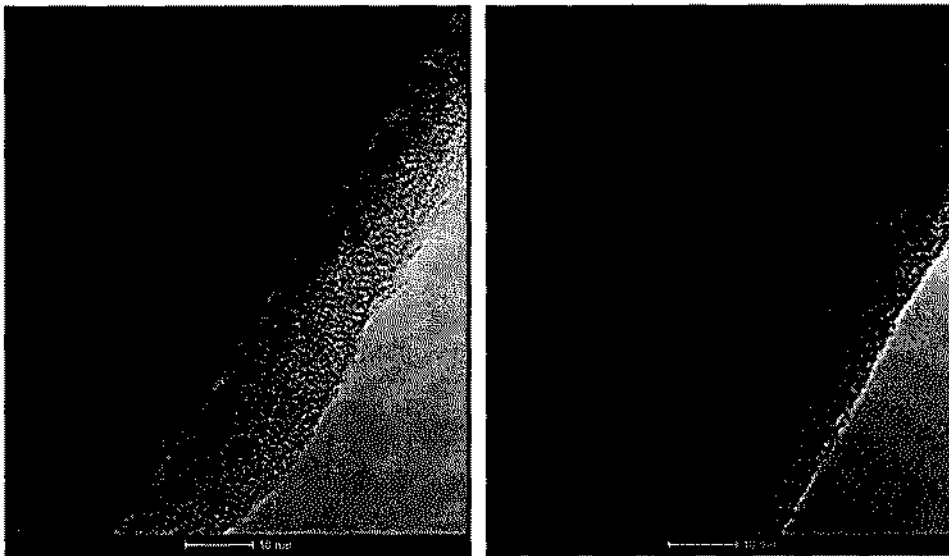
Figure 4.5: HRTEM images of Carbon implanted BNNTs: (a) and (b) Both with a resolution of 10nm.

Structure of boron nitride nanotubes changes with ion dose application. With increasing the ion dose, structural deformation goes on increasing. Amorphization of the outer core increases as the structural disorder increases under the effects of ion beam with a high dose 5×10^{14} ions.cm^{-2} [120]. Some darker spots and holes are also visible on the surface. However heating effects of incoming ion beam should be cautiously taken into account [109].
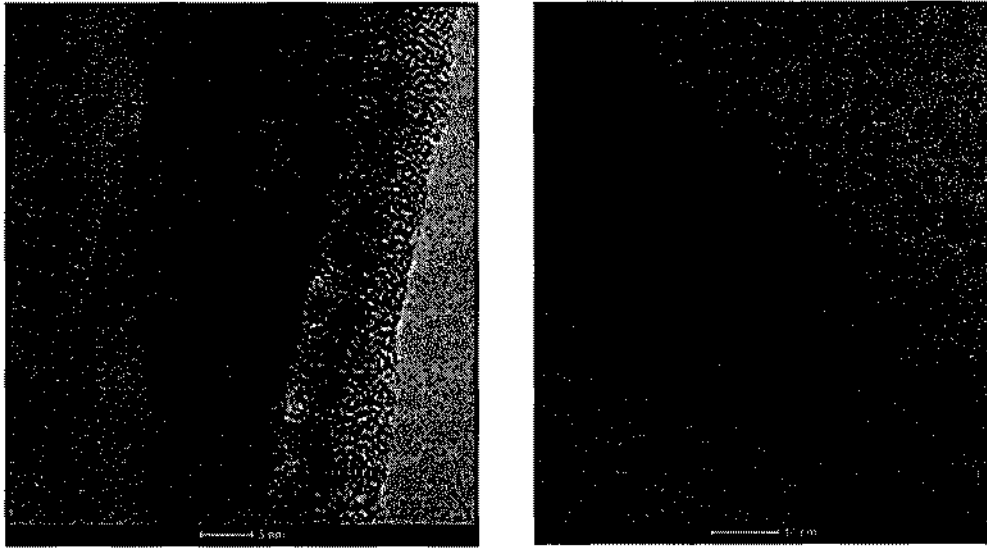
Figure 4.6: HRTEM images of implanted BNNTs at a high dose with a resolution of (a) 5nm (b) 10nm.

4.2 Structural Investigation

4.2.1 X-Ray Diffraction Studies

X-Ray diffraction patterns were recorded at 25^0C with diffractometer employing CuKα
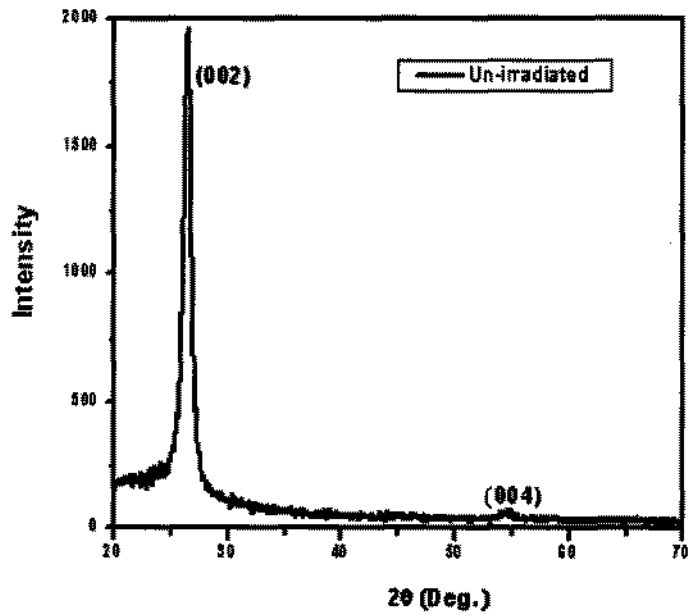
Figure 4.7: XRD patterns of Un-irradiated h-BNNTs .

radiation. XRD pattern for un-irradiated nanotubes suggests that nanotubes are well crystallized along <002> orientation. We observe visible diffraction peaks at $2\theta = 26.2$, and 54.7, which could be attributed to h-BNNTs (002) and (004) planes of h-BN respectively [110]. After ion irradiation, C doping is successfully achieved and for a dose of 10^{12} ions.cm^{-2} visible diffraction peaks appear at $2\theta = 26.2$, 42.3 and 54.7 corresponding to h-BCN (002), (100) and (004) planes respectively [111].
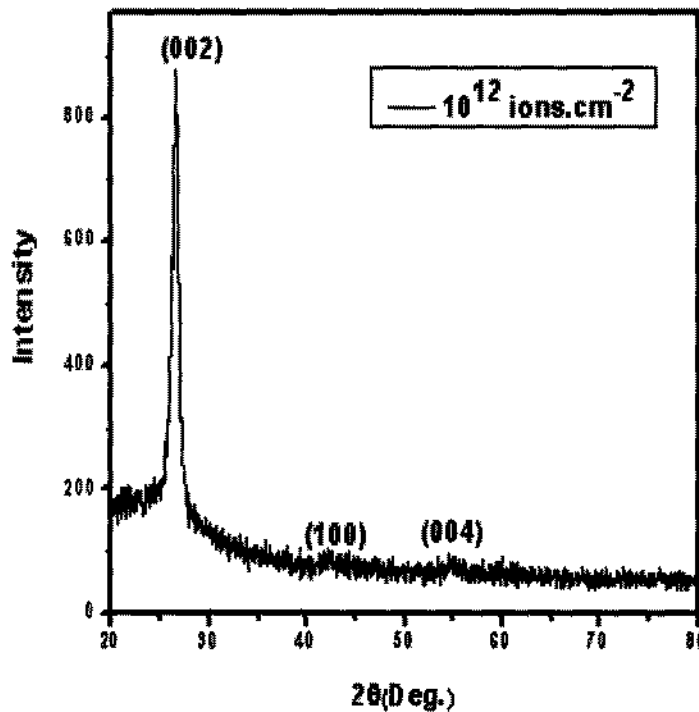
Figure 4.8: XRD patterns of h-BNNTs at ion dose of 10^{12} ions.cm^{-2}

XRD analysis of h-BNC at a dose of 10^{13} ions.cm^{-2} and 5×10^{14} ions.cm^{-2} depicts that by applying a heavy ion dose nanotubes become amorphous [120]. In both of these cases nanotubes are well crystallized along <002> orientation, some other peaks with very low intensity appear but reduction of intensity and broadening of peaks suggests lack of crystallization [83].
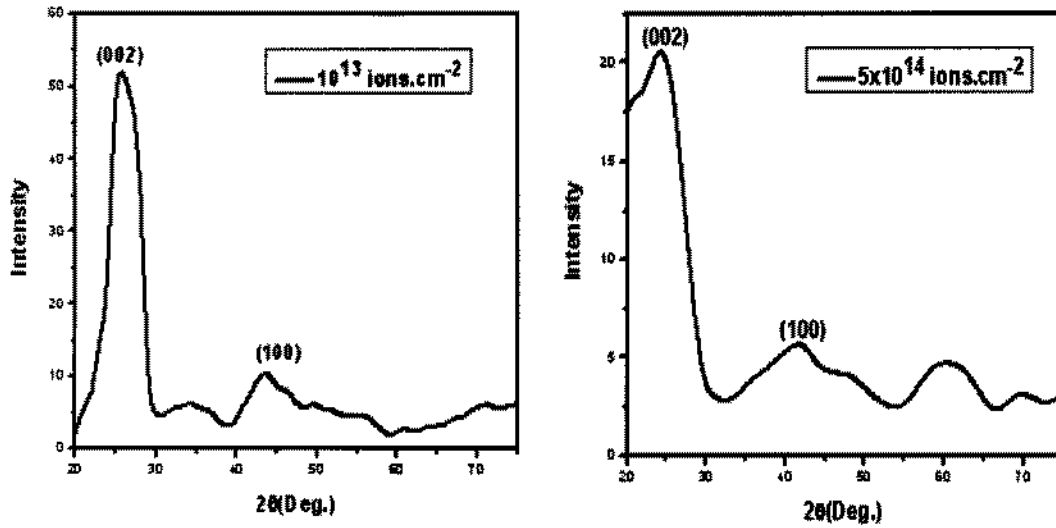
Figure 4.9: XRD patterns of h-BNNTs at ion dose of (a) 10^{13} ions.cm^{-2} (b) 5×10^{14} ions.cm^{-2}.

4.3 Composition Spectroscopy

4.3.1 Non-Rutherford Backscattering Spectroscopy (NRBS)

Non-Rutherford backscattering analysis technique was employed using 5UDH Tandem accelerator. Beam of α-particles (He^{++} ions) with an ion beam energy of 4.25 MeV and beam current of 15nA were allowed to fall on boron nitride nanotubes spread over the glass substrate with an incident angle of 0°. Backscattered particles were collected at an angle of 170°. This technique is used for mass and depth resolution in C^{+} implanted boron nitride nanotubes. Compositional information obtained from the collected backscattered particles confirms the successful implantation of carbon in boron nitride nanotubes. At a dose of 5×10^{14} ions.cm^{-2} carbon peak becomes significantly apparent whereas boron and nitrogen were already the constituents of nanotubes. Some other peaks such as calcium, sodium, silicon and oxygen also appear in the spectra that belong to composition of glass which is used as a substrate in each case [64, 65].

61
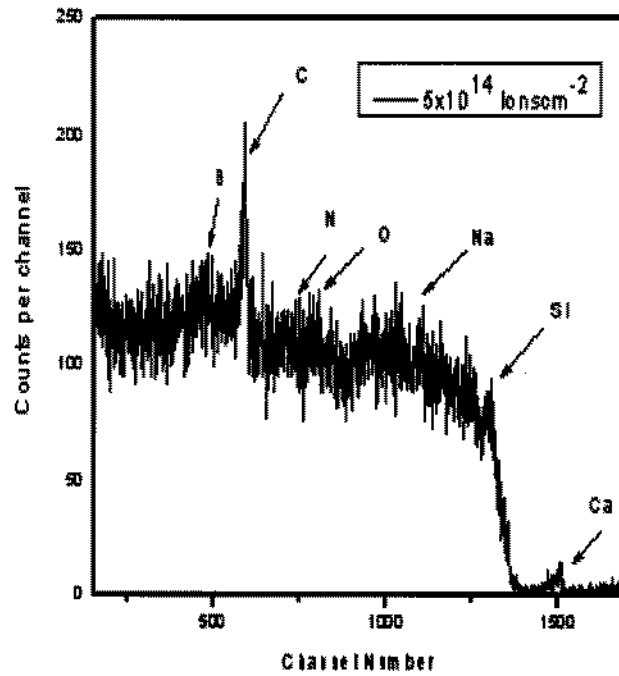
Figure 4.10: Non-Rutherford Backscattering studies of carbon implanted Boron Nitride Nanotubes at a heavy ion dose.
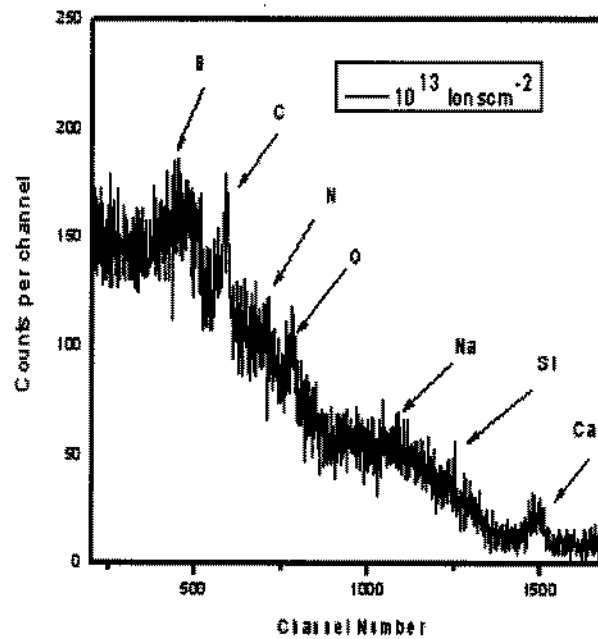
Figure 4.11: Non-Rutherford Backscattering studies of carbon implanted Boron Nitride Nanotubes at a dose of 10^{13} ions.cm^{-2}.

Carbon ions were also implanted in boron nitride nanotubes at low dose of 10^{13} ions.cm^{-2} and 10^{12} ions.cm^{-2}. Non-Rutherford backscattering profile shows carbon peaks in the spectrum in both the cases. Backscattered yield suggests that carbon content is large in the case of high ion dose of 5×10^{14} ions.cm^{-2} and decreases as the ion dose decreases (Figure 4.10 and 4.12).
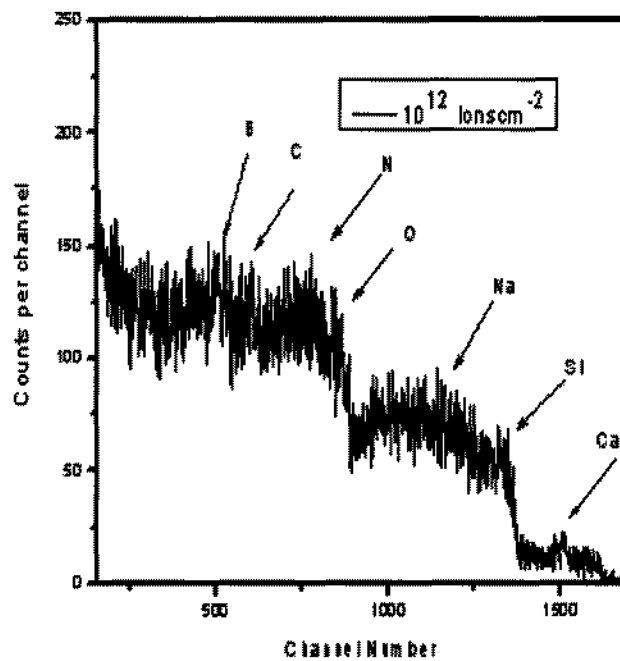
Figure 4.12: Non-Rutherford Backscattering studies of Carbon implanted Boron Nitride Nanotubes at a dose of 10^{12} Ions.cm^{-2} showing compositional profile.

4.4 Vibrational Spectroscopy

4.4.1 Infrared Spectroscopy

Ion implanted samples were analyzed by using Infrared spectroscopy with Nickolet 6700 FTIR. In un-irradiated nanotubes, three different peaks appear. B-N in-plane stretching gives rise to a peak at 771 cm^{-1} in the IR spectra. When B-N-B bond bends out of the plane, another peak at 1380cm^{-1} is observed. Both of these are characteristic modes of h-BNNTs (figure 4.13). Peak between 2200cm^{-1} and 2300cm^{-1} belongs to Boron [112].

63
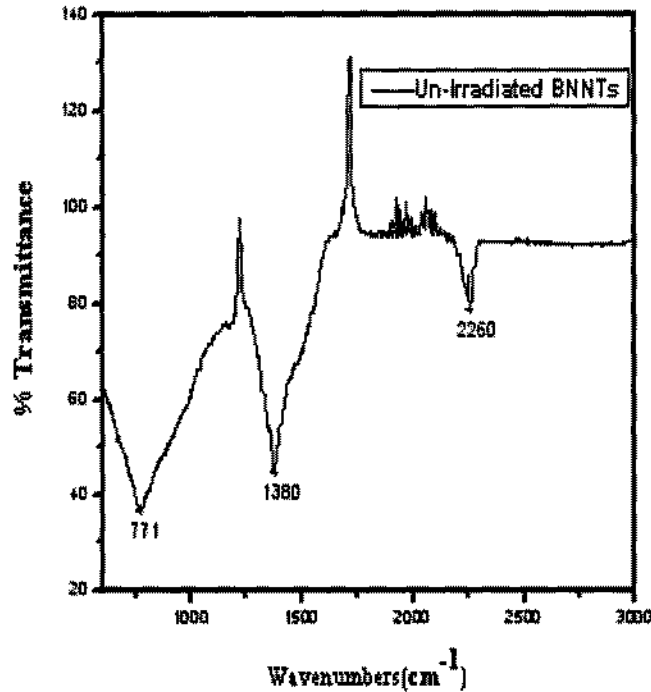
Figure 4.13: Infrared spectroscopy of hexagonal Boron Nitride Nanotubes showing bonds between nitrogen and boron.

When a heavy dose of carbon ions $5x10^{14}$ ions.cm^{-2} is applied on BNNTs, a relatively large amount of carbon is implanted in the nanotubes. A large narrow peak at 889cm^{-1} show that carbon makes bonds with nitrogen and substitutes boron atoms in the nanotubes (Figure 4.14). Although some carbon ions replace nitrogen atoms and make bond with Boron, as the B-C vibrational mode appears at 1000cm^{-1}[113]. When nanotubes were analyzed with IR spectroscopy after irradiation of carbon ions with 10^{13} ions.cm^{-2} dose, C-N and B-C bonds vibrate and their modes of vibrations give rise to two additional peaks at 889 cm^{-1} and 997 cm^{-1} respectively. Other peaks at 779cm^{-1} and 1370 cm^{-1} belong to stretching vibrations of B-N. Peak at 2250cm^{-1} belongs to boron. At a dose 10^{12} ions.cm^{-2}, vibration modes of C-N and B-C are observed at 883cm^{-1} and 1000 cm^{-1}. These peaks again confirm the presence of carbon content in h-BNNTs, Thus carbon has been successfully implanted even at a low dose 10^{12} ions.cm^{-2} [110].
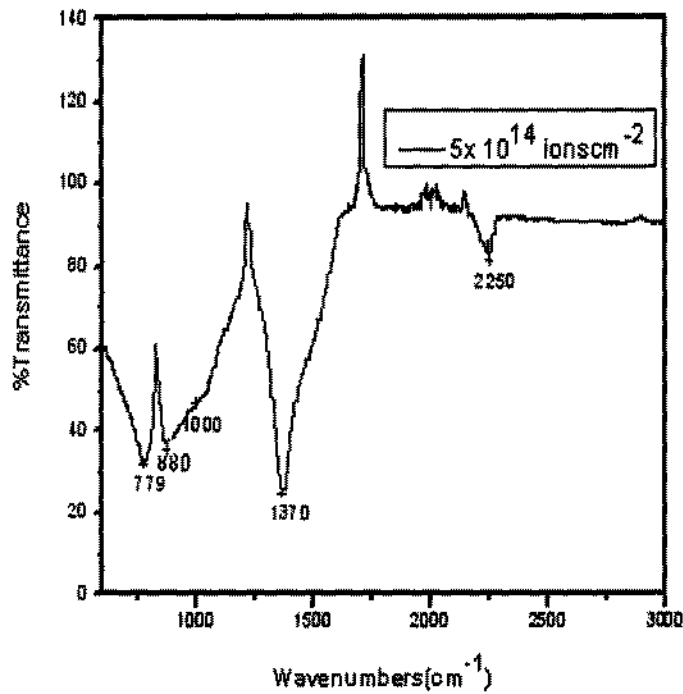
Figure 4.14: Infrared spectroscopy of Boron nitride Nanotubes implanted at ion dose of $5x10^{14}$ ions.cm^{-2}.

Peak intensity for C-N mode is small as compared to other two cases which employs that carbon content is very small as this fact is already observed with non-Rutherford backscattering analysis. B-N peaks move are proposed to lower energy shift that can be due to stress relief after carbon doping [113-115]. Formation of hybrid ternary BCN nanostructure is confirmed by bonding mechanism. Infrared Spectra shows that carbon is making bond with nitrogen and boron, thus carbon replaces boron and nitrogen species and makes bonds in the lattice.
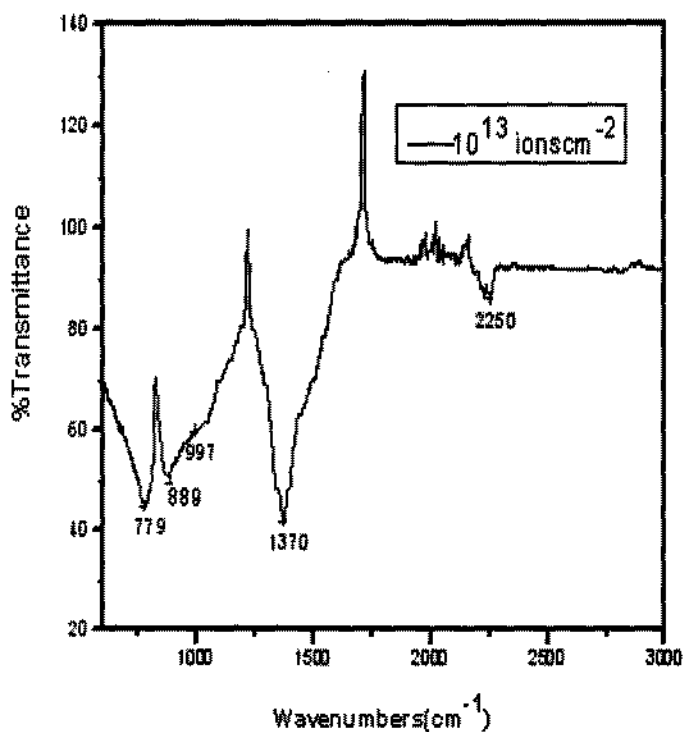
Figure 4.15: Infrared spectroscopy of Boron nitride Nanotubes implanted at 10^{13} $ions.\,cm^{-2}$ dose showing C-N, B-C, B-N-B and B-N bonds in the h-BNNTs.
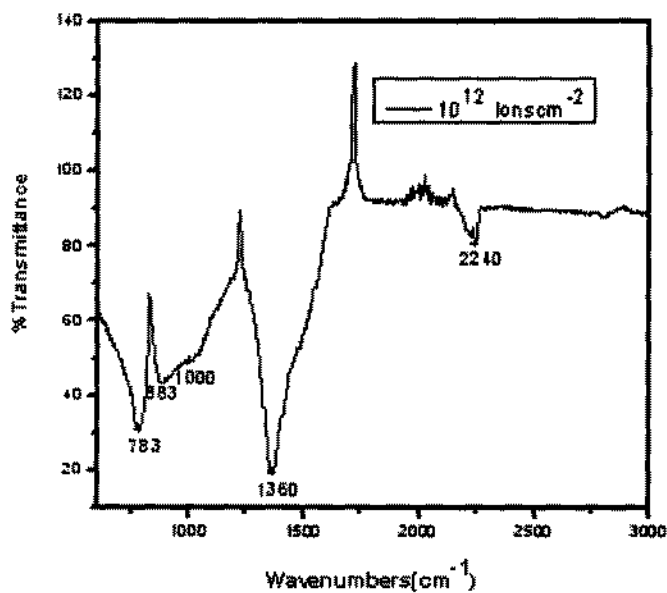
Figure 4.16: Infrared spectroscopy of Boron nitride Nanotubes irradiated with a low dose of 10^{12} $ions.cm^{-2}$, showing B-C and C-N bonds.

66

4.4.2 Raman Spectroscopy

Raman spectra of nanotubes were recorded before and after carbon implantation. Peak at 1367cm^{-1} in Raman spectra of un-irradiated tubes corresponds to h-BN Raman active mode, derived from in plane displacements of boron and nitrogen atoms toward each other [111, 116].
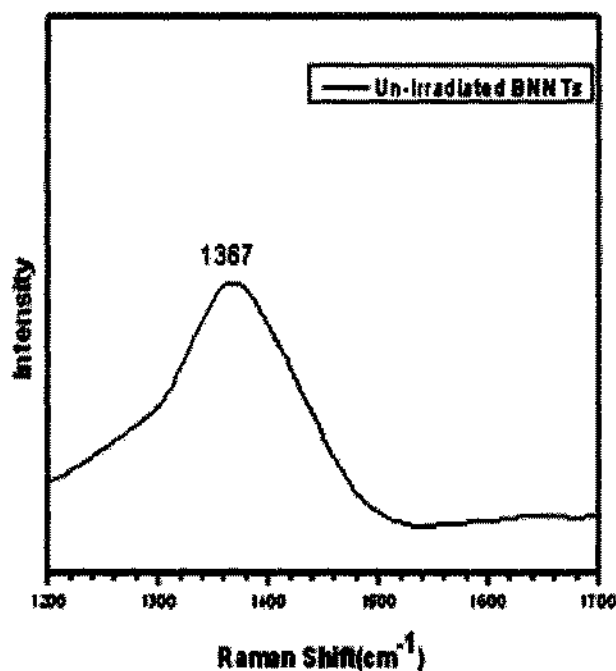
Figure 4.17: Raman studies of Nanotubes before irradiation.

After irradiation, ions are successfully implanted in BNNTs as Raman peaks corresponding to h-BNC structure are observed. As in Figure 4.18, with ion dose value of 10^{12} ions.cm^{-2} , peak at 1372 cm^{-1} belong to D-band of h-BNC. This peak is subjected to a high energy shift. An additional peak appears in the spectra at 1579 cm^{-1} which belongs to G-band of h-BNC [116]. Some other unknown broad peaks having low intensity also appear in the Raman spectra, which may be due to irradiation effects. Since the ion implantation of h-BNNTs has not been performed before this attempt, thus these peaks have not been found in literature.

67
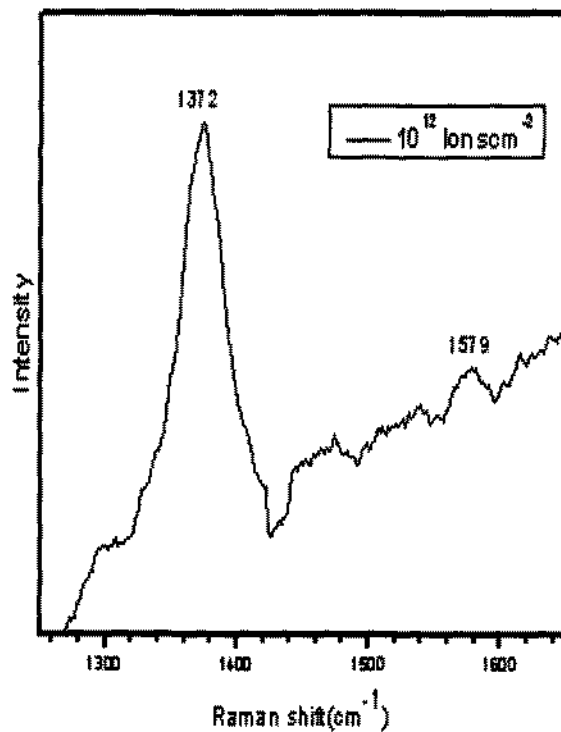
Figure 4.18: Raman studies of Nanotubes after irradiation of 10^{12} ions.cm^{-2}.

At a dose of 10^{13} ions.cm^{-2}, two peaks corresponding to G-band and D-band of h-BNC appear at 1594cm^{-1} and 1374 cm^{-1} respectively. Similarly at a high dose of 5×10^{14} ions.cm^{-2}, two peaks appear at 1379 cm^{-1} and 1598cm^{-1} attributed to h-BNC D-band and G-band respectively. It is observed that irradiated BNNTs depict higher energy shift as compared to un-irradiated nanotubes. This energy shift is due to a decrease in average bond length which is caused by incorporation of C atom whose covalent radius is smaller than B atoms. As the concentration of carbon atoms in nanotubes increases, larger energy shift is observed [116-119].
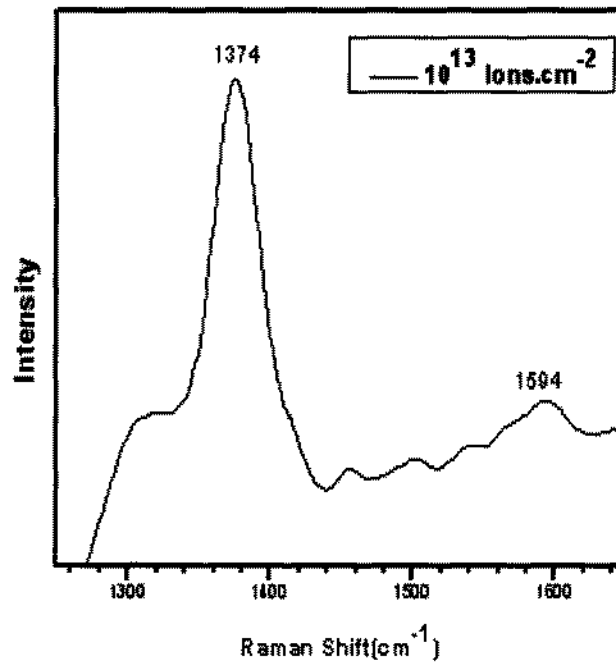
Figure 4.19: Raman studies of Boron Nitride Nanotubes irradiated at a dose of 10^{13} Ions.cm^{-2}
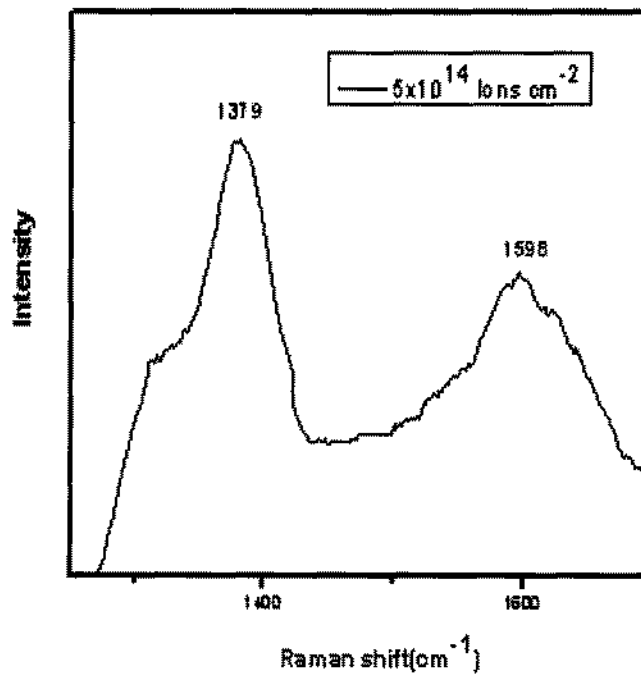
Figure 4.20: Raman studies of Boron Nitride Nanotubes irradiated at a dose of 5×10^{14} Ions.cm^{-2}.

69

4.5 Optical Studies

4.5.1 UV- Absorption Spectroscopy

The results of absorption spectroscopy were conducted by using UV-spectrophotometer. Four samples of h-MWBNNTs were prepared. One of the samples was kept un-irradiated. Other three samples were irradiated with ion doses $5x10^{14}$ ions.cm^{-2}, 10^{13} ions.cm^{-2} and 10^{12} ions.cm^{-2}. These h-MWBNNTs with band gap energy of 5.5eV were irradiated with ion beam energy of 0.8MeV. Results of absorption spectroscopy of un-irradiated and ion implanted h-MWBNNTs reveal that the energy gap decreases with an increase in C ions concentration.
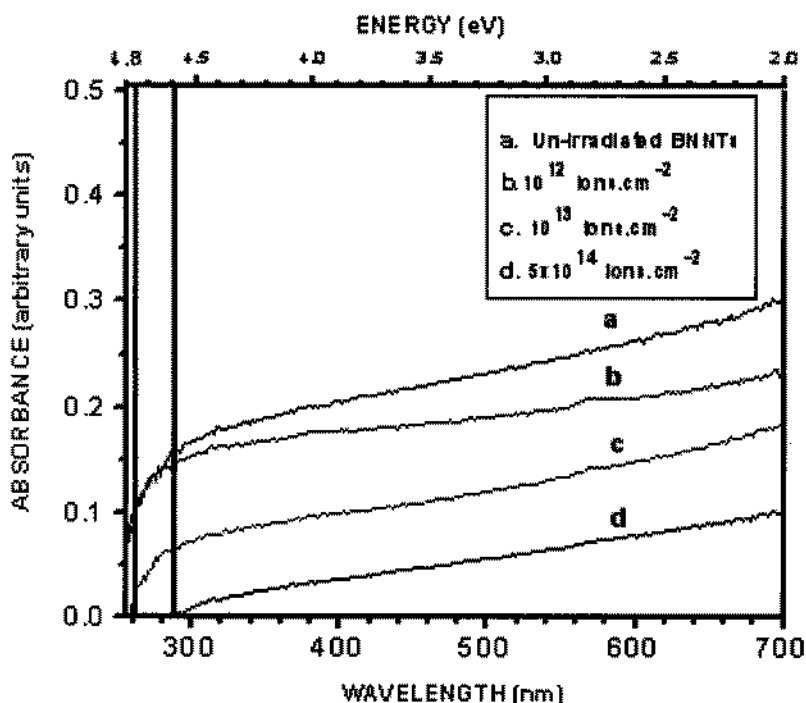
Figure 4.21: Results of UV-absorption spectroscopy of h-BNNTs at different ion doses show an effect of carbon concentration on the bandgap of h-BNNTs.

As shown in Figure 4.21, at a heavy ion dose of $5x10^{14}$ ions.cm^{-2}, energy band is decreased to 4.6eV due to C^{+} implantation. At a dose of 10^{13} ions.cm^{-2}, band gap is found to be 4.8eV.Similarly at a low dose of 10^{12} ions.cm^{-2} band gap is reduced to

4.9eV. Band gap of un-irradiated nanotubes is 5.5 eV. After ion implantation, band gap is reduced by 0.9 eV and a crossover from insulator to conductor is observed. Resulting boron carbonitride nanotubes show a reduction in band gap that can be attributed to reduction in π-bonding states due to incorporation of C atoms in BNNTs. As we keep on increasing the carbon content in BNNTs, a newly derived energy band appears around the center of band gap of BNNTs. Newly derived energy band belongs to C atoms, which effectively reduces the bandgap of BNNTs [34]. BCN nanotubes exhibit semiconducting behavior which can be tuned with the quantity of carbon content. It is theoretically predicted that carbon doping in BN lattice gives either electron carriers or hole carriers [41].
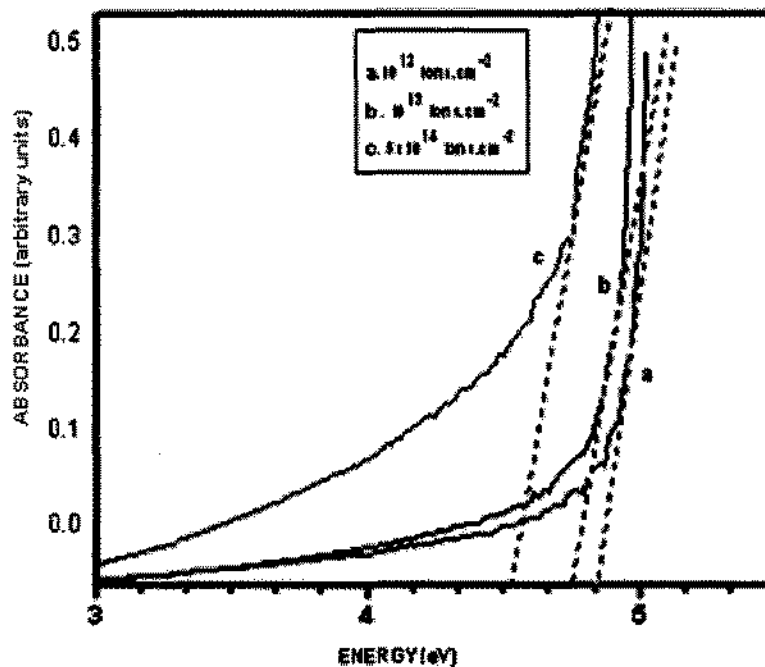
Figure 4.22: Bandgap energy versus absorption graphs showing bandgap significantly tuned to 4.6eV at a dose of 5×10^{14} ions.cm^{-2}.

If boron is substituted by carbon, we are left with excess of electrons. If carbon substitutes nitrogen site, then we are left with holes. Substitutional doping determines whether the nanotubes are n-type or p-type. Thus a change in electronic properties is observed [51, 110]. Band gap of BNNTs is found to be inversely proportional to carbon content [111].

CONCLUSIONS

- Carbon ion implantation of hexagonal multiwalled boron nitride nanotubes was successfully performed using 5-UDH Tandem accelerator with ion beam energy of 0.8MeV.

- Effects of ion implantation under different ion doses were studied using NRBS, XRD, FTIR, SEM, absorption spectroscopy, SEM and HRTEM analysis.

- NRBS confirmed that carbon is successfully implanted. Moreover, FTIR analysis confirmed that carbon is making bonds with boron and nitrogen. Carbon substitutes boron atoms and makes bond with nitrogen. Hence carbon doping resulted in the formation of boron carbonitride nanotubes (BCNNTs), which is one of the frontier carbon materials.

- Bandgap of boron nitride nanotubes was sufficiently reduced by carbon substitutional doping. Reduction in the bandgap was found to be inversely proportional to carbon content. BNNTs turned from insulator to n-type semiconductor.

- XRD and HRTEM analysis showed that crystallinity of the nanotubes decreases with an increase in ion dose. Outer core of nanotubes gets amorphous at a high ion dose due to formation of defects, thus providing a two way electronic path.

- Raman spectra show a decrease in average bond length due to incorporation of C atoms whose size is greater than B atoms.

RECOMMENDATIONS

- Effects of annealing on carbon implanted products can be studied. Annealing can reduce defects as well as good electrical performance is expected after annealing.

- Different types of ions can be implanted in BNNTs such as silicon ions can be implanted in BNNTs, which is expected to bring photonics and optoelectronics revolution.

- Effects of temperature during ion implantation can be varied, which can result in successful implantation with controlled defects.

- Magnetic behavior of nanotubes can be studied after ion irradiation.

- Electrical performance of amorphous BCN nanotubes can be studied.

- Ion implantation mechanism can be used for implantation of various other nanostructures

REFERENCES

[1] Norio Taniguchi, "On the basic concept of nano-technology", Proc. Int. conf. Prod. Eng. Tokyo, 18-23, 1974.

[2] Nanotechnology, http://publications.nigms.nih.gov/chemhealth/cool.htm.

[3] J.J.Ramdsen, "What is nanotechnology", Nanotech. Perceptions, 1, 3-17, 2005.

[4] The nanotube site, http://www.pa.msu.edu/cmp/csc/nanotube.html.

[5] L.A. Girifalco, M.H., et al., "Carbon nanotubes, buckyballs, ropes and a universal graphitic potential", Phys. Rev. B, 62, 13104-13110, 2000.

[6] Raymond M. Reilly, "Carbon Nanotubes: Potential Benefits and Risks of Nanotechnology in Nuclear Medicine", J. Nucl. Med., 48(7), 1039-1040, 2007.

[7] Michael S. Starno. C.A., et al., "Electronic structure control of single-walled carbon nanotube functionalization", Science, 301(5639), 1519-1522, 2003.

[8] Karin Gos, Interaction between parallel carbon nanotube quantum dots, page 97-98, (2011).

[9] A carbon nanotube page, http://www.personal.reading.ac.uk/~scsharip/tubes.htm.

[10] Lijima, "Helical microtubules of graphitic carbon", Nature, 354, 56-57, 1991.

[11] Lijima, Ichihashi, "Single-shell carbon nanotubes of 1-nm diameter", Nature, 363, page 603, 1993.

[12] Bethune, D.S., Kiang, de Varies, "Cobalt- catalysed growth of carbon nanotubes with single-atomic-layer walls", Nature, 363, 605-609, 1993.

[13] Michael S. Starno. C.A., et al., "Electronic structure control of single-walled carbon nanotube functionalization", Science, 301(5639), 1519-1522, 2003.

[14] L.A. Girifalco, M.H., et al., "Carbon nanotubes, buckyballs, ropes and a universal graphitic potential", Phys. Rev. B, 62, 13104-13110, 2000.

[15] A. S. Milev, G. S. K. Kannangara, "Nanotechnology", Kirk-Othmer Encyclopedia of chemical technology, 17, 1-29, 2005.

[16] Properties and applications of carbon nanotubes, http://www.cheaptubes.com/carbon-nanotubes-101.htm.

[17] R.H.Baughman, A.A.Zakhidov, "Carbon nanotubes-the route toward applications", Sci. Comp. Rev: Botany, 297, 787-791, 2002.

REFERENCES

[18] Ado jorio and Gene Dresselhaus, Carbon nanotubes: Advanced topics in synthesis, structure, properties and applications, pages 421-436, (2008). http://en.wikipedia.org/wiki/Potential_applications_ of_carbon_nanotubes.

[19] L. Vel., et al., "Cubic boron nitride: Synthesis, physicochemical properties and applications", Mater. Sci. Engi: B, **10**, 149-164, 1991.

[20] Laetitia Vaccarini, C. Goze, et al.," Mechanical and electronic properties of carbon and boron nitride nanotubes", Carbon, **38**, 1681-1690, 2000.

[21] Boron nitride: hexagonal structures, http://www.britannica.com.

[22] A. Kelly, K.M. Knowles, "Crystallography and crystal defects", page 97, (2012).

[23] Yoke khin yap, "B-C-N Nanotubes and related nanostructures", Lec. Note. Nano. Sci. Tech, **6**, 84-87, 2011.

[24] Dmitri Golberg, Yoshio Bando, Yang Huang, Z. Xu, et al., "Recent Advances in Boron Nitride Nanotubes and Nanosheets", Isr. J. Chem, **50**, 405–416, 2010.

[25] Electrical properties of Boron nitride nanotubes, http://www.dummies.com.

[26] Blase, Rubio, Cohen, M.L., et al., "Stability and band gap constancy of Boron nitride nanotubes", Europhys.lett, **28**, 335-340, 1994.

[27] Santosh, et al., "Elastic properties of Boron nitride nanotubes and their comparison with Carbon nanotubes", J. Nanosc.nanotech,**9**, 5425-5430, 2009.

[28] D.Golberg, Y.B., et al., "Boron nitride nanotubes", Adv.mater., **19**, 2413-2432, 2007.

[29] D.Golberg, P.C., et al., "Direct force measurements and kinking under elastic deformation of individual Multiwalled boron nitride nanotubes", Nano lett.,**7**, 2146-2151, 2007.

[30] Chen, Campbell, J., et al., "Boron nitride nanotubes: pronounced resistance to oxidation", Appl.Phys.Lett, **84**, 2430-2432, 2004.

[31] (a). Kim, P., Shi, L., M., A., et al., "Thermal Transport Measurements of Individual Multiwalled Nanotubes" Phys. Rev.Lett., **87**, 2155021-4 (2001). (b) Duclaux, L., Nysten, B., et al., "Thermal Conductivity of Copoly (ethylene vinyl acetate)/Nano-filler Blends", Phys.Rev.B, **46**, 3362-3367, 1992.

[32] Laude, et al., "Boron nitride nanotubes grown by non-ablative laser heating: synthesis, characterization and growth processes", Phd thesis, 2001.

75

REFERENCES

[33] Mauricio Terrones, N.G., et al., "Synthetic routes to nanoscale $B_xC_yN_z$ architectures", Carbon, **40**, 1665-1684, 2002.

[34] Y.D.Peng, L.Y.A., et al.," Chemical synthesis and characterization of flaky h-BCN at high pressure and high temperature", Chin.Phys.Lett., **24**, 1088-1091, 2007.

[35] P.Piquini, R.J.Bairele, et al., "Formation energy of native defects in BN nanotubes: an ab initio study", Nanotechnology, **16**, 827-831, 2005.

[36] J. L. He, "Chemical synthesis of crystalline hexagonal B-C-N compound", J. Mater. Sci. lett., **19**, 2061-2063, 2000.

[37] Khin et al., Lecture Notes in Nanoscale Science and Technology, page 1-22, 2009.

[38] O.Stephen, P.M.Ajayan, C.C., et al., "Doping graphitic and carbon nanotube structures with Boron and nitrogen", Science, **266**, 1683-1685, 1994.

[39] Mpourmpakis, G., et al., "Why boron nitride nanotubes are preferable to carbon nanotubes for hydrogen storage? An ab initio theoretical study", Catalys.today, **120**, 341-345, 2007.

[40] L.Liao, K.L., et al., "Multiwalled Boron carbonitride/Carbon nanotube junction and its Rectification Behavior", J. Am. Chem. Soc., **129**, 9562–9563, 2007.

[41] Kalyan R., D.J., et al., "Synthesis, structure and properties of homogenous BC_4N nanotubes", J. mater.chem., **18**, 83-90, 2007.

[42] A. A. Koos, F.D., et al., "Comparison of structural changes in nitrogen and boron doped Multiwalled carbon nanotubes", **48**, 3033-3041, 2010.

[43] J. L. He, "Chemical synthesis of crystalline hexagonal B-C-N compound", J.Mater.Sci.lett., **19**, 2061-2063, 2000.

[44] F.Piazza, J.E.Nocua, A.H., et al., "Formation of boron carbonitride nanotubes from in situ grown carbon nanotubes", Dia. Rel. Mater, **14**, 965-969, 2005.

[45] C. V. Zhi, X. D. Bai., et al., "Resonance Raman scattering of Boron carbonitride nanotubes", Appl. phys. lett., **84**, 1549, 2004.

[46] L.Luo, L. Mo, et al., "Facile synthesis of Ternary Boron Carbonitride Nanotubes", Nanoscale Res. Lett., **4**, 834-838, 2009.

[47] K. Suenaga, C. C., et al., "Synthesis of nanoparticles and nanotubes with well-separated layers of Boron nitride and carbon", Science, **278**, 653-655, 1997.

REFERENCES

[48]   C.V.Zhi, X.D.Bai., et al., "Resonance Raman scattering of Boron carbonitride nanotubes", Appl.phys.lett., **84**, 1549, 2004.

[49]   W.L. Wang, X.D. Bai, et al.,"Direct synthesis of B-C-N single-walled nanotubes by bias-assisted hot filament chemical vapor deposition", J. Am. Chem. Soc.,**128**,6530-6531, 2006.

[50]   Xianlong Wei, M.S. Wang, et al., "Electron-beam-induced substitutional carbon doping of boron nitride Nanosheets, nanoribbons, and nanotubes" ACS Nano, **5**, 2916–2922, 2011.

[51]   Chopra, N. G., Luyken, et al., "Boron nitride nanotubes", Science, **269**, 966-967, 1995.

[52]   Loiseau, A., Williaime, et al., " Boron nitride nanotubes with reduced numbers of layers synthesized by arc discharge", Phys. Rev. Lett.,**76**, 4737-4740, 1996.

[53]   Terrones, M., et al., "Metal particles catalysed production of nanoscale BN nanostructures", Chem.Phys.Lett., **259**, 568-574, 1996.

[54]   Golberg, D., Bando, et al., "Nanotubes in boron nitride laser heated at high pressure", Appl. Phys. Lett., 69, 2045-2047, 1996.

[55]   Wengsieh, Z., Cherrey , et al., "Synthesis of $B_xC_y N_z$ nanotubes", Phys. Rev. B, **51**, 11229-11232, 1995.

[56]   Zhang, Y., Gu, H., et al., "Heterogeneous growth of B-C-nanotubes by laser ablation, Chen. Phys. Lett., **279**, 264-269, 1997.

[57]   Terrones, M., et al., "Pyrolytically grown $B_xC_yN_z$ nanomaterials: nanofibers and nanotubes", Chem. Phys. Lett., **257**, 576-582, 1996.

[58]   J.L.He, "Chemical synthesis of crystalline hexagonal B-C-N compound", J.Mater.Sci.lett., **19**, 2061-2063, 2000.

[59]   Sen, R., et al., "B-C-N, C-N and B-N nanotubes produced by the pyrolysis of precursor molecules over Co catalysts", Chem. Phys. Lett., **287**, 671-676, 1998.

[60]   Kohler-Redlich, Ph., Terrones, M., et al., "Stable BC2N nanostructures: low temperature Production of segregated C/BN layered materials", Chem. Phys. Lett., **310**, 459–465, 1999.

[61]   Jilin Wang, Y. Yu, et al., "Synthesis of boron nitride nanotubes by self-propagation high-temperature synthesis and annealing method", J. Nanomater., **2010**, 1155-1161, 2010.

[62]   R. S. Wagner and W.C. Ellis, "Vapor-liquid-solid mechanism of single crystal growth", Appl. Phys. Lett., 4(5), 88-90, 1964.

[63]   T.J. Trentler, K. M. Hickman, et al., "Solution-liquid-solid growth of crystalline III-V semiconductors: an analogy to vapor-liquid-solid growth", Science, 270, 5243, 1791-1794, 1995.

[64]   The chemistry of glass, http://simon-davies.suite101.com

[65]   Glass composition,http://gpi.org/glassresources/education/sustainabilityrecycling/section-24-glass-composition.html.

[66]   Pelletron Accelerator, http://www.pelletron.com/charging.htm.

[67]   Tandem Particle Accelerator, http://www.britannica.com/EBchecked/media/59812/Two-stage-tandem-particle-accelerator-A-beam-of-negative-ions.

[68]   Tandem accelerator at National Centre for Physics, http://www.ncp.edu.pk/epd.

[69]   O'Keefe, M.A., P.R., et al., "Computed crystal structure images for high resolution electron microscopy", Nature, 274(5669), 322-324, 1978.

[70]   Williams, David B., Transmission electron microscopy: A text book of material science, second edition, Page 91-110, 2009.

[71]   Ludwig Reimer and Helmut Kohl, Transmission Electron Microscope, fifth edition, Page 3-4, 2008.

[72]   Transmission Electron Microscope, http://en.wikipedia.org/wiki/Transmission_electron_microscope.

[73]   Higher Resolution Transmission Electron Microscope, http://en.wikipedia.org/wiki/High-resolution_transmission_electron_microscopy.

[74]   L. Reimer, Scanning Electron Microscopy, second edition, Pages 13,57, (1998).

[75]   Scanning Electron Microscopy, http://serc.carleton.edu/research_education/geochemsheets/techniques/SEM.html.

[76]   What is the SEM? , http://www-archive.mse.iastate.edu/microscopy/whatsem.html.

[77]   Option from Quanta to Quarks, http://webs.mn.catholic.edu.au/physics/emery/hsc_quanta_quarks.htm.

[78]   X-Ray Diffraction, http://serc.carleton.edu/research_education/geochemsheets/techniques/XRD.html.

[79]   Bragg's Law, http://www.britannica.com/EBchecked/topic/76973/Bragg-law.

REFERENCES

[80] X-Ray Diffraction Techniques, http://encyclopedia2.thefreedictionary.com.

[81] Kazuto Yamauchi, et al., "Single-nanometer focusing of hard X-rays by Kirkpatrick-Baez mirrors", J. Phys: Condens. matter, **23**, 394206, 2011.

[82] P. Harold, X-ray diffraction procedures for polycrystalline and amorphous materials, second edition, Page 270-295, (1977).

[83] B. D. Cullity, Elements of X-ray Diffraction, Pages 420-426,(1977).

[84] C. Giacovazzo, Fundamentals of Crystallography, second edition, Page 530, (2002).

[85] P. Harold, X-ray diffraction procedures for polycrystalline and amorphous materials, second edition, Pages 270-295, (1977).

[86] B. E. Warren, X-ray Diffraction, second edition, page 15-27, (1969).

[87] Tapash R. Rautray , R. N., et al., "Ion implantation of Titanium based biomaterials", Pro. Mater. Sci., **56**, 1137-1177, 2011.

[88] Baoxia Mi, Orlando Coronell , B. J. Marinas, et al., " Physico-chemical characterization of NF/RO membrane active layers by Rutherford Backscattering Spectroscopy", J. Memb. Sci., **282**, 71-81, 2006.

[89] Rutherford Backscattering of thin films,http://cnx.org/content/m22411/latest.

[90] Zeev B. Alfassi and Max Peisach, Elemental analysis by Particle accelerators, Pages 180-219, (1992).

[91] H. R. Verma, Atomic and Nuclear analytical Methods, Page 91-140, (2007).

[92] Fourier Transform infrared spectroscopy, http://mmrc.caltech.edu/FTIR/FTIRintro.pdf.

[93] Attenuated Total Reflection,
http://shop.perkinelmer.com/content/technicalinfo/tch_ftiratr.pdf .

[94] IR Spectroscopy, http://en.wikipedia.org/wiki/File:IR_spectroscopy_apparatus.jpg.

[95] Raman Spectroscopy Basics,
http://content.piacton.com/Raman_Spectroscopy_Basics.pdf.

[96] What is Raman Spectroscopy, http://www.inphotonics.com/raman.htm.

[97] Even Smith and Geoffrey Dent, Modern Raman Spectroscopy, Page 60-78, (2005).

[98] Laser Raman Spectroscopy,
http://www.chm.bris.ac.uk/pt/diamond/stuthesis/chapter2.htm.

[99] Maher S. Amer, Raman spectroscopy, fullerenes and nanotechnology, Pages 43-58, (2008).

REFERENCES

[100] John R. Ferraro and Kazuo Nakamoto, Introductory Raman Spectroscopy, Second Edition, page 22-26, (2003).

[101] Michael J. K Thomas and David J. Ando, Ultravoilet and Visible spectroscopy, Page 45- 50, (1996).

[102] B. J. Clark and T. Frost, UV Spectroscopy: Techniques, Instrumentation, Data Handling, First Edition, Page 6-23, (1993).

[103] Multiwalled Boron Nitride Nanotubes: Growth, Properties and Applications, http://www.springer.com/978-1-4419-0085-2.

[104] Duangkamon Baowan, B. j. Cox, et al., "Junctions between a boron nitride nanotubes and a boron nitride sheet", Nanotechnology, **19**, 075704-075716, 2008.

[105] A. Ishaq, L. Yan, J. L. Gong, et al., "Multi-walled carbon nanotubes under N ion beam irradiation", Nanoelect. Conf. second IEEE Intl., 945-947, 2008.

[106] Z Ni, Q Li, L Yan, J Gong, et al., "Welding of multi-walled carbon nanotubes by ion beam irradiation", Carbon, **46**, 376-378, 2008.

[107] Jilin Wang, Y. G., et al., Synthesis of boron nitride nanotubes by self-propagation high-temperature synthesis and annealing method", J. Nanomater., **2010**, 540456-540462, 2010.

[108] T. M. Schmidt, R. J. Baierle, et al.,"Theoratical study of native defects in BN nanotubes", Phys. Rev B, **67**,113407, 2003.

[109] Ossi Lehtinen, T. K. N., et al., "Ion irradiation of multi-walled boron nitride nanotubes", Phys. Status Solidi C, 7(no: 3-4), 1256-1259, 2010.

[110] Y. D. Peng, L.Y.A., et al.," Chemical synthesis and characterization of flaky h-BCN at high pressure and high temperature", Chin. Phys. Lett., **24**, 1088-1091, 2007.

[111] C. Y. Zhi, J. D. Guo, et al, "Adjustable boron carbonitride nanotubes", J. Appl. Phys., **91**, 5325-5333, 2002.

[112] D. He, W. Cheng, et al., "Relief of the internal stress in ternary boron carbonitride thin films", Appl. Surf. Sci., **191**, 338-343, 2002.

[113] S. Fahy, C. A. Taylor, et al., "Islanding and stain-induced shifts in the infrared absorption peaks of cubic boron nitride thin films", Phys. Rev. B, **56**(19), 125963, 1997.

[114] Didem Ozmen, Production and characterization of Boron nitride nanotubes, PhD thesis, Middle East University, 2008.

REFERENCES

[115] Ludger Wirtz and Angel Rubio, Optical and vibrational properties of boron nitride nanotubes, http://nano-bio.ehu.es/files/articles/Wirtz_2009_430.pdf.

[116] C. Y. Zhi, X. D. Bai, and E. G. Wang, "Raman characterization of boron carbonitride nanotubes", Appl. Phys. Lett. **80**, 3590-5392, 2002.

[117] Yong Jae Cho, Chang H. K., et al., "Electronic structure of Si-doped BN nanotubes using X-Ray photoelectron spectroscopy and first principle calculation", Chem.Mater., **21**(1), 136-143, 2009.

[118] Tetsuya Kida, K. Shigezumi, et al.,"Synthesis of boroncarbonitride (BCN) films by plasma enhanced chemical vapor deposition using trimethylamine borane as a molecular precursor", Vacuum, **83**, 1143-1146, 2009.

[119] A. V. Krasheninnikov and K. Norlund, "Ion and electron irradiation-induced effects in nanostructured materials", J. Appl. Phys. Rev, **107**(6), 071301, 2007.

[120] Ossi Lehtinen, Irradiation effects in graphene and related materials, Phd Thesis, University of Helsinki Finland, 2011.